Heinrich Event Intercomparison with the ice-sheet model SICOPOLIS

(氷床モデル SICOPOLIS を用いたハインリッヒ・イベントの数値実験およびモデル間相互比較)

Ryoji Takahama

Master's thesis

Hokkaido University

Graduate School of Environmental Science

2006

Abstract

Heinrich events (HEs) are large scale surges of the Laurentide Ice Sheet (LIS) over Hudson Bay and Hudson Strait. These surges are thought to be triggered by the internal dynamics of the ice sheet. Therefore it is important to investigate HEs in order to estimate the effect on climate variability.

It will be tested whether the 3D ice sheet model SICOPOLIS is able to simulate such large scale surges, and what is their sensitivity to change in surface and basal boundary conditions. The model domain is a flat horizontal square. The ice sheet is built up from zero ice thickness over 200 ka, with a temporally constant glacial-climate forcing. The bedrock elevation remains flat throughout the simulations. Further, the geothermal heat flux is applied directly at the bottom of the ice sheet.

We could generate many saw-shape oscillations of the ice sheet expressing a series of growth phases and HEs from the standard run. The growth time is about 7 ka, whereas the subsequent HE collapse lasts only for several hundred years.

Parameter studies showed that surface temperature affects the ice volume, and surface accumulation affects the periodicity of HEs. Further, the strength of the subglacial sediment affects the amplitude of ice-volume changes. Therefore, surface and basal conditions of the LIS are crucial elements for HEs.

Acknowledgement

Without support of many people, this thesis could not have been realized.

I did not have any knowledge about geoscience, glaciology and computer before I started my study in Graduate School of Environmental Science Hokkaido University. I cannot put my thanks for **Prof. Ralf GREVE** in words. His advice and suggestive discussion on my study have helped me significantly. I got a lot of knowledge about dynamics of glaciers and ice-sheets, climate variability of the earth and international communication skills in his classes and through discussion with him. **Prof. Takeo HONDOH** gave me a kind of philosophy. **Prof. Takayuki SHIRAIWA** provided on opportunity for field work on a glacier and guided the direction of master thesis. **Dr. Shin SUGIYAMA** taught me ice-sheet dynamics and gave me suggestions on my study and my master thesis. I had helpful discussions on my work with **Dr. Akira HORI. Dr. Atsushi MIYAMOTO, Dr. Shinichiro HORIKAWA, Dr. Junichi OKUYAMA, Dr. Hiroshi OHNO, Dr. Isenko EVGENY,** and **Dr. Tetsuo SUEYOSHI,** and they supported my daily life. I express my sincere gratitude to **Kaori KIDAHASHI** for her patient support and encouragement for my study. I am grateful to **Hakime SEDDIK, Syousaku KANAMORI,** and **Teppei J. YASUNARI** for their hearty warm cheering. Last, but not least, I thank **all staff and colleagues** of Institute of Low Temperature Science.

Contents

1. General introduction

1.1 Influence of ice sheets on climate

Ice sheets influence climate because they are they are among the largest topographic features on the planet, create some of the largest regional anomalies in albedo and radiation balance, and represent the largest readily exchangeable reservoir of fresh water on the earth. Variations in freshwater fluxes from ice sheets are especially large, because although ice sheets grow at the usually slow rate of snowfall, they shrink at the faster rate of surface melting, or the even faster rate of surface of ice-sheet dynamics (surging). As they grow and shrink, ice sheets reorganize continental drainage by damming rivers or reversing river flow through isostatic bedrock depression under the ice, creating lakes that fill over years to centuries but that may drain an order or orders of magnitude faster when ice dams fail [Hays et al., 1976].

Statistical analysis of paleoclimate data support the Milankovitch theory of glaciation driven by orbital changes by showing that Northern Hemisphere ice sheets have waxed and waned with the same periods [100, 41, and 23 thousand years] as the orbital parameters (eccentricity, obliquity, precession) that control the seasonal distribution of insolation at high northern latitude [Walder and Costa., 1992]. Other features of the climate system also show these orbital periodicities, but many lag insolation forcing of climate change at high northern latitudes by much longer (from 5 to 15 thousand years, depending on the period) than expected [Imbrie et al., 1992, 1993]. Because ice sheets are one of the few components of the climate system with a time constant of this length, they may have been responsible for amplifying and transmitting changes that correspond to orbital periodicities in high latitude seasonality elsewhere through the climate system with a phase lag corresponding to their long time constant. According to this hypothesis,

interactions among Northern Hemisphere ice sheets and other features of the climate system thus translate high latitude insolation forcing into a global climate signal with dominant orbital-scale glaciation cycles (from 10^4 to 10^5 years) in which millennial-scale variations (from 10^3 to 10^4 years) are embedded [Bond et al., 1993].

Millennial-scale (10^3-year) climate variations during the glaciations mainly consist of two dominant modes, Dansgaard-Oeschger (D/O) cycles, with an approximate spacing of 1500 years, and Heinrich Events (HEs), with a longer variable spacing (from 10^3 to 10^4 years) [Bond et al., 1993; Bond et al., 1999]. The D/O oscillation is an oceanic process, often triggered by meltwater changes [Keigwin et al., 1991]. Most HEs involve surging of the LIS through Hudson Strait, apparently triggered by D/O cooling [Bond et al., 1993; Bond et al., 1999]. The icebergs released to the North Atlantic during a HE cause a near shutdown in the formation of NADW [Keigwin and Lehman., 1984].

1.2 Introduction of HEs

1.2.1 Discovery of HEs

A German Oceanographer, Hartmut Heinrich, studied the responses of the earth systems to the orbital forces from the sea sediment. He concentrated on the land rocks layers which are included in sediment cores drilled from the North Atlantic. In 1988, he published the results of this study, and showed that these rock layers were derived from huge collapses of icebergs which were launched from Canada into the North Atlantic. As they melted, they released land rocks that were dropped into the grained sediments on the ocean floor. Much of this ice rafted debris consists of limestone very similar to those exposed over large areas of eastern Canada today [Heinrich., 1988].

After his discovery, many sea sediment cores were drilled from the North Atlantic (Deep Sea Drilling Project). Six Heinrich layers were identified, which extend 3000 km across the North Atlantic, almost reaching Ireland [Kawakami., 1995].

1.2.2 Relation between HEs and climate changes

High resolution studies of ocean cores have now revealed that the iceberg calving events occurred even more frequently at intervals of 2 to 3 thousand years (see Fig. 1.1) between 10 thousand years and 38 thousand years ago. A plot of the amount of rock fragments obtained from the samples (Fig 1.1, left panel) shows the youngest 4 HEs and 10 subsidiary peaks which are derived from smaller surges. The proportion of the left hand coiled variety of the foraminifera (*Neogloboquadrima pachyderma*) (Fig. 1.1, right panel) indicates warm and cold conditions. Cold surface waters are characterized by fossil foraminifera assemblages containing over 90 per cent of sinistral *N.pachyderma*.

Some of these events were shown to be related to changes in surface water temperatures as determined by the proportion of foraminifera. Many of the peaks in the occurrence of rock fragments shown in Figure 1.1 coincide with >90 per cent proportions of the cold water foraminifera.

This shows that the release of iceberg collapse coincided with low North Atlantic sea surface temperatures, indicative of stadial periods, which were followed by rapid warming into interstadials. As wee will see in Figure 1.2, these temperature changes are paralleled by temperature changes detected in cores drilled at the Greenland ice sheet.

Ice coring began in Greenland in the late 1970s, but only in the early 1990s were two holes drilled to the bedrock near the summit of the ice dome. The first borehole to reach bedrock was that undertaken by the European funded Greenland Ice-core Project (GRIP).

The plot of δO_{18} from the GRIP core reveals 24 interstadials, 21 of which are shown in Figure 1.2. The repeated episodes of rapid warming/cooling are known as D/O events after their discoverers. They start with rapid increases in temperatures over the Greenland ice sheet that occurred over a hundred years or less. Relatively slower cooling then follows until the next warming

event.

These shorter events are bundled together into longer cooling cycles (from 7 to 13 thousand years) characterized by steady drops between successive peaks in the δO_{18} values. These bundles are known as Bond cycles after their discoverer and are shown in Figure. 1.2 as saw-shaped lines. The large ice rafted debris peaks at the end of each Bond cooling cycle are HEs. The cooling trend through each Bond cycle may have been caused by the downwind effect from the growth of the LIS. The mechanism of HEs at the end of each cycle will be discussed in section 1.2.3.

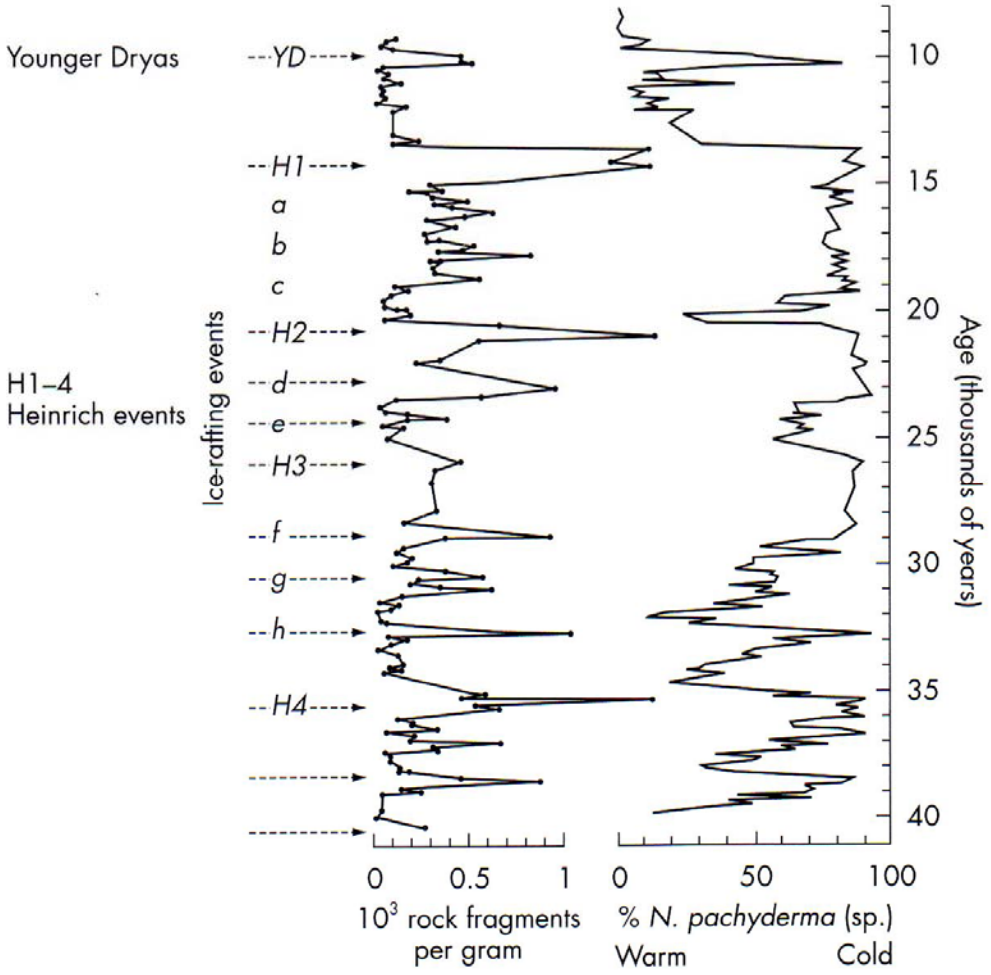

Fig. 1.1: Evidence for North Atlantic iceberg collapses [Bond et al., 1995].

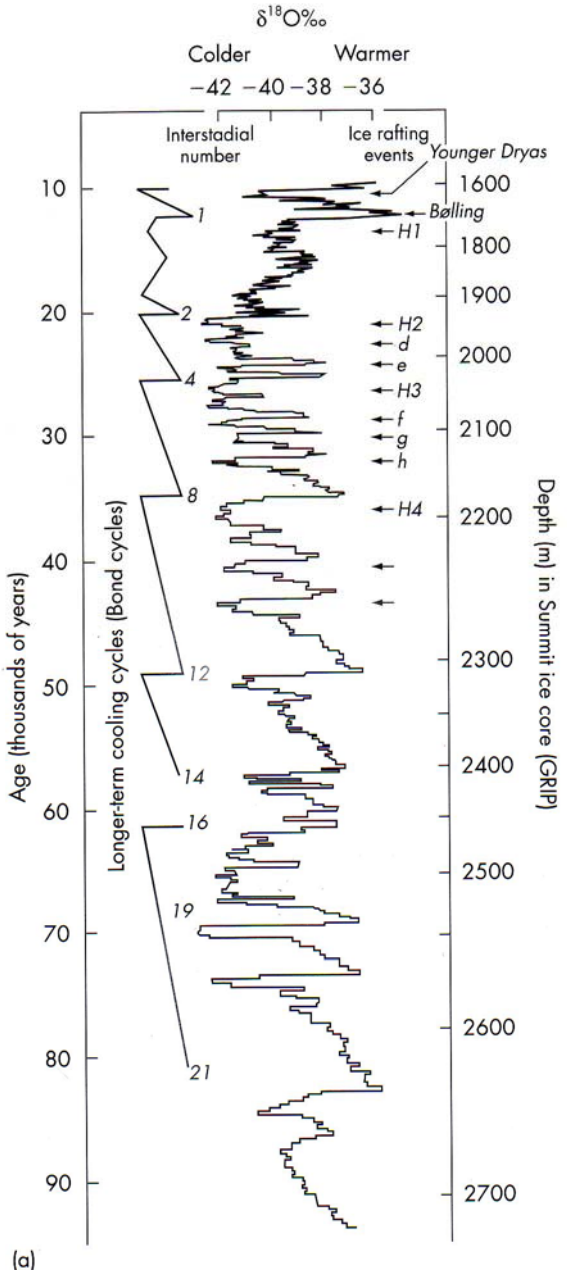

Fig. 1.2: D/O and Bond cycles in the GRIP ice core [Bond et al., 1993].

1.2.3 Mechanism of HEs

Clearly HEs resulted from periodic surges in the flow of the ice sheet covering eastern Canada, but were these surges triggered by climatic changes, or by the dynamics of the ice sheet which resulted in surging unconnected to links between ice, the atmosphere and/or the oceans? The nature of the differences between these two models, known respectively as the MacAyeal (or 'binge-purge' model) and Denton model, are shown in Figure 1.3.

In the MacAyeal model (or 'binge-purge' model), the cause of HEs is the internal instabilities of the LIS. As the LIS gets thicker because of snowfall, the stronger insulation effect traps more heat. Then the basal temperature rises gradually until the pressure melting point. When the basal temperature reaches pressure melting, the melted subglacial sediment lubricates and a large-scale surge (HE) occurs.

On the other hand, in the Denton model, the cause of HEs is the external force. The global cooling harmonizing with the orbital movements causes ice sheet and/or ice shelf expansion.

There are two problems in the Denton model. First, the slow response of the ice sheet to the climate change. The transmission of the ice sheet surface changes to the base takes about 1-10 thousand years, but the interval of the ice sheet collapses which are recorded in the sea sediments is about 2 to 3 thousand years. Second, the HEs do not have a regular cycle. If the external force is the main cause of HEs, the calving would supply icebergs to the North Atlantic regularly because the climate obeys the orbital forces.

On the other hand, the MacAyeal model (or 'binge-purge' model) can explain rapid initiation and termination of HEs, and explain the varying time between the HEs (7-13 thousand years) as this will be dependent on the size of the ice sheet.

In conclusion, the internal ice sheet dynamics seems to be more appropriate

as the main cause for HEs than the external forcing. It is important to investigate HEs in terms of glaciology as well as of climatology (R. Willson., 2000).

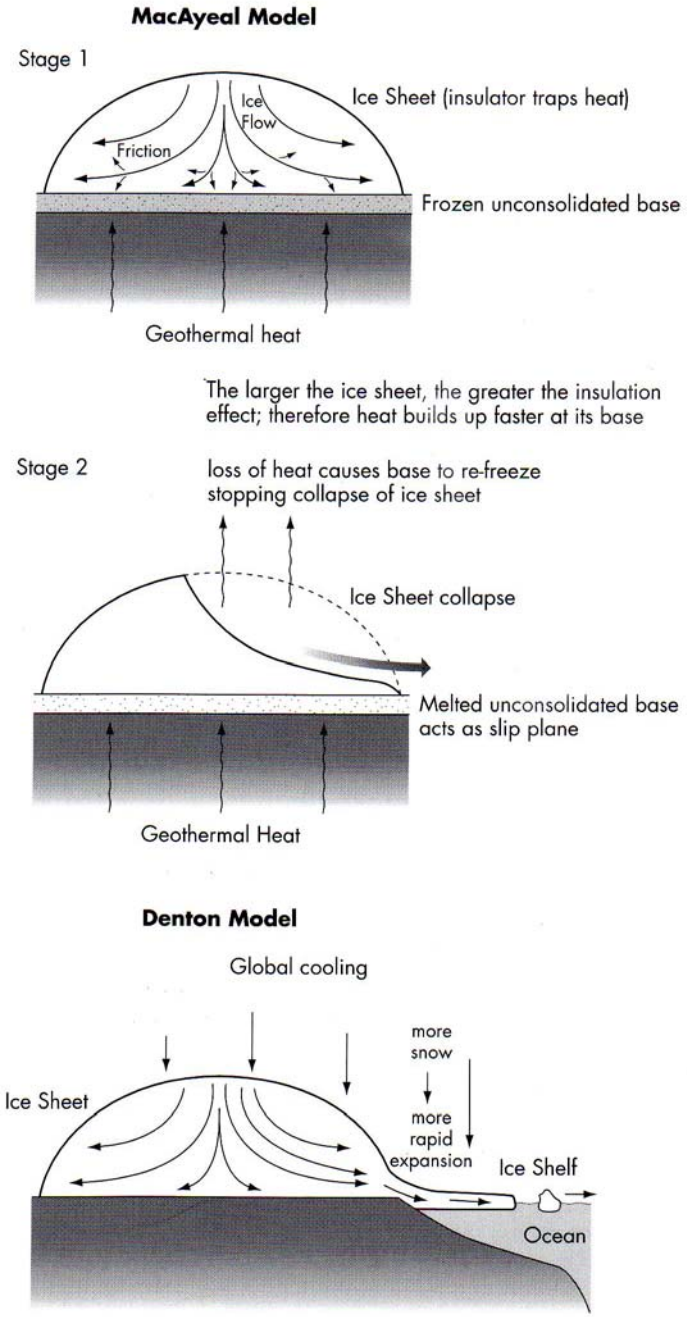

Fig. 1.3: Sketches showing the features of the MacAyeal and Denton models for the origin models of HEs [by M. Maslin].

2 Ice-sheet dynamics and thermodynamics

2.1 Balance equations

Ice is treated as incompressible viscous fluid. Mass, momentum and energy balance equations are

$$\nabla \cdot \boldsymbol{v} = 0 , \tag{1}$$

$$\rho_I \frac{d\boldsymbol{v}}{dt} = \nabla \cdot \boldsymbol{\sigma} + \rho_I \boldsymbol{g} , \tag{2}$$

$$\rho_I \frac{d(cT)}{dt} = \nabla \cdot k_I \nabla T + \Phi . \tag{3}$$

Here, $\boldsymbol{v}$ is the velocity vector, ρ_I the ice density, t the time, $\boldsymbol{\sigma}$ the stress tensor, $\boldsymbol{g}$ the gravity acceleration vector, c the specific heat capacity of ice, k_I the thermal conductivity of ice and Φ the strain heating. The continuity equation (1) expresses the conservation of mass of ice. The right-hand side is equal to zero because the density of ice is not considered to be changed. Three dimensional stress balances for each part of the material are described by the momentum balance equation (2). The energy equation (3) describes the total energy within ice (Greve., 2004 / 2005).

2.2 Ice flow

Ice sheets are assumed to be in a quasi-steady state on a long time scale (e.g., ≥ 1 kyr), which means that the acceleration term in Eq. (2) is neglected. Explicitly, using $\boldsymbol{g} = (0,0,-g)$, Eq. (2) becomes,

$$\frac{\partial \sigma_{xx}}{\partial x} + \frac{\partial \sigma_{xy}}{\partial y} + \frac{\partial \sigma_{xz}}{\partial z} = 0, \tag{4a}$$

$$\frac{\partial \sigma_{yx}}{\partial x} + \frac{\partial \sigma_{yy}}{\partial y} + \frac{\partial \sigma_{yz}}{\partial z} = 0, \tag{4b}$$

$$\frac{\partial \sigma_{zx}}{\partial x} + \frac{\partial \sigma_{zy}}{\partial y} + \frac{\partial \sigma_{zz}}{\partial z} = \rho_I g, \tag{4c}$$

where σ_{ij} are the stress components in a three dimensional field (see Fig. 2.1). Ice velocity is calculated from a constitutive equation, which relates the deviatoric stress tensor $\boldsymbol{\sigma}'$, and strain-rate tensor D, through the following equation;

$$D_{ij} = EA(T')\tau_e^{n-1}\sigma'_{ij}, \tag{5}$$

where the stress-deviator components σ'_{ij} are obtained by subtracting the amplitude of the hydrostatic pressure (the mean normal stress) from the stress components,

$$\sigma'_{ij} = \sigma_{ij} - \frac{1}{3}\delta_{ij}\sum_k \sigma_{kk}. \tag{6}$$

Eq. (5) is called "Glen's flow flow", in which the strain rate is proportional to the (n-1)-th power of effective shear stress τ_e, the ice temperature dependent factor, *A(T')* (*T'* is the temperature relative to pressure melting, also called the homologous temperature) and the factor of other effects, *E*. The factor *E* is called enhancement factor, which controls the softness of ice and implicitly reflects the effect of impurity and/or anisotropy. Although the form of the relation is well-established and can be explained in terms of dislocation theory, it is essentially an empirical fit to laboratory and field data for the loading conditions and stresses encountered in glaciers.

The strain rate is explicitly expressed by the spatial derivatives of the velocity components as follows,

$$D_{ij} = \frac{1}{2}\left[\frac{\partial v_i}{\partial x_j} + \frac{\partial v_j}{\partial x_i}\right] \quad (i,\ j = 1,\ 2,\ 3), \tag{7}$$

or in components,

$$\begin{pmatrix} \dot{D}_{xx} & \dot{D}_{xy} & \dot{D}_{xz} \\ \dot{D}_{yx} & \dot{D}_{yy} & \dot{D}_{yz} \\ \dot{D}_{zx} & \dot{D}_{zy} & \dot{D}_{zz} \end{pmatrix} = \begin{pmatrix} \dfrac{\partial u}{\partial x} & \dfrac{1}{2}\left[\dfrac{\partial u}{\partial y} + \dfrac{\partial v}{\partial x}\right] & \dfrac{1}{2}\left[\dfrac{\partial u}{\partial z} + \dfrac{\partial w}{\partial x}\right] \\ \dfrac{1}{2}\left[\dfrac{\partial v}{\partial x} + \dfrac{\partial u}{\partial y}\right] & \dfrac{\partial v}{\partial y} & \dfrac{1}{2}\left[\dfrac{\partial v}{\partial z} + \dfrac{\partial w}{\partial y}\right] \\ \dfrac{1}{2}\left[\dfrac{\partial w}{\partial x} + \dfrac{\partial u}{\partial z}\right] & \dfrac{1}{2}\left[\dfrac{\partial w}{\partial y} + \dfrac{\partial v}{\partial z}\right] & \dfrac{\partial w}{\partial z} \end{pmatrix}. \tag{8}$$

The effective shear stress τ_e is defined as the second invariant of the stress deviator,

$$\tau_e^2 = \frac{1}{2}\sum_{i,j}\left(\sigma'_{ij}\right)^2 = \frac{1}{2}\left[\left(\sigma'_{xx}\right)^2 + \left(\sigma'_{yy}\right)^2 + \left(\sigma'_{zz}\right)^2\right] + \left(\sigma_{yz}\right)^2 + \left(\sigma_{zx}\right)^2 + \left(\sigma_{xy}\right)^2. \tag{9}$$

Everywhere in an ice sheet except for the immediate vicinity (some 10 km horizontal distance) of ice domes (local maxima of the surface elevation h) and ice margins, the flow regime is essentially simple, bed-parallel shear, and the slopes of the free surface and the ice base are small (Fig. 2.2). The internal horizontal velocity v_x, v_y can be calculated by using Eq. (4) ~ (9) with the stress-free condition at the surface, and simplifications of the stress field called shallow ice approximation (SIA),

$$v_{h,x} = -2(\rho g)^n \,|\mathrm{grad}h|^{n-1} \frac{\partial h}{\partial x}\int_b^z EA(T')(h-\tilde{z})^n d\tilde{z}, \tag{10a}$$

$$v_{h,y} = -2(\rho g)^n \,|\mathrm{grad}h|^{n-1} \frac{\partial h}{\partial y}\int_b^z EA(T')(h-\tilde{z})^n d\tilde{z}. \tag{10b}$$

The entire horizontal velocity can then be calculated by adding the velocity at the ice base into (10),

$$v_x = v_{b,x} - 2(\rho g)^n \,|\mathrm{grad}h|^{n-1} \frac{\partial h}{\partial x}\int_b^z EA(T')(h-\tilde{z})^n d\tilde{z}, \tag{11a}$$

$$v_y = v_{b,y} - 2(\rho g)^n \, |\mathrm{grad} h|^{n-1} \, \frac{\partial h}{\partial y} \int_b^z EA(T')(h - \tilde{z})^n \, d\tilde{z} \,. \qquad (11b)$$

For expressions of the basal velocity see below (Sect. 2.4).

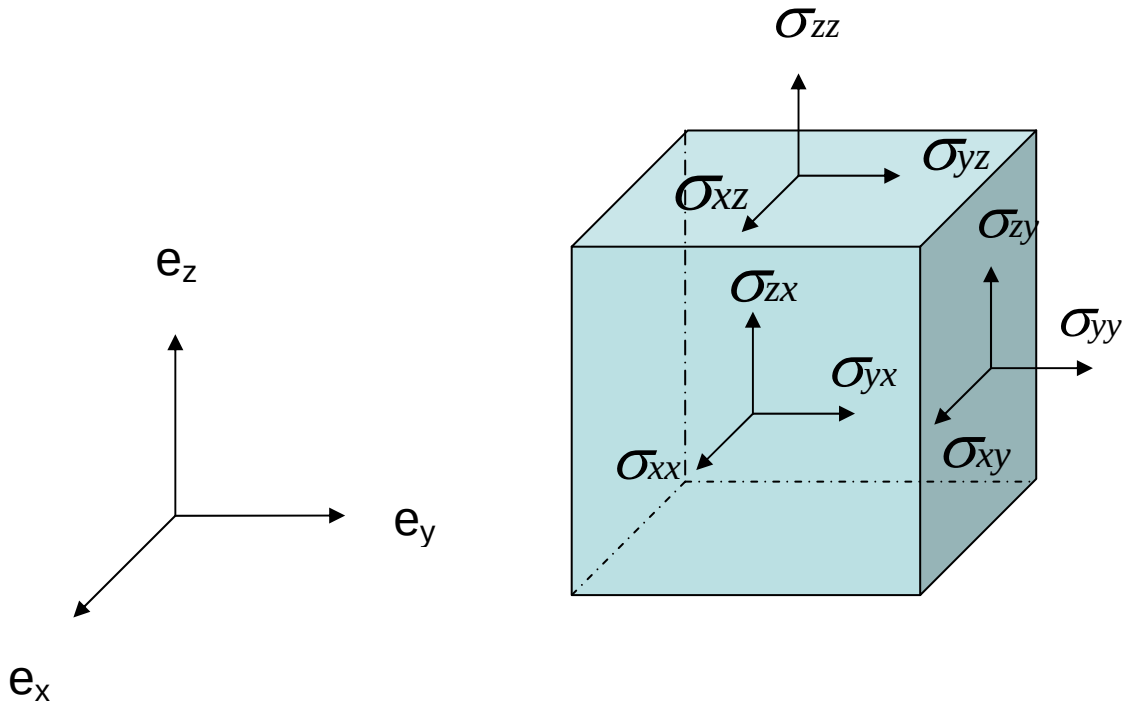

Fig. 2.1: Stress components in a three dimensional field.

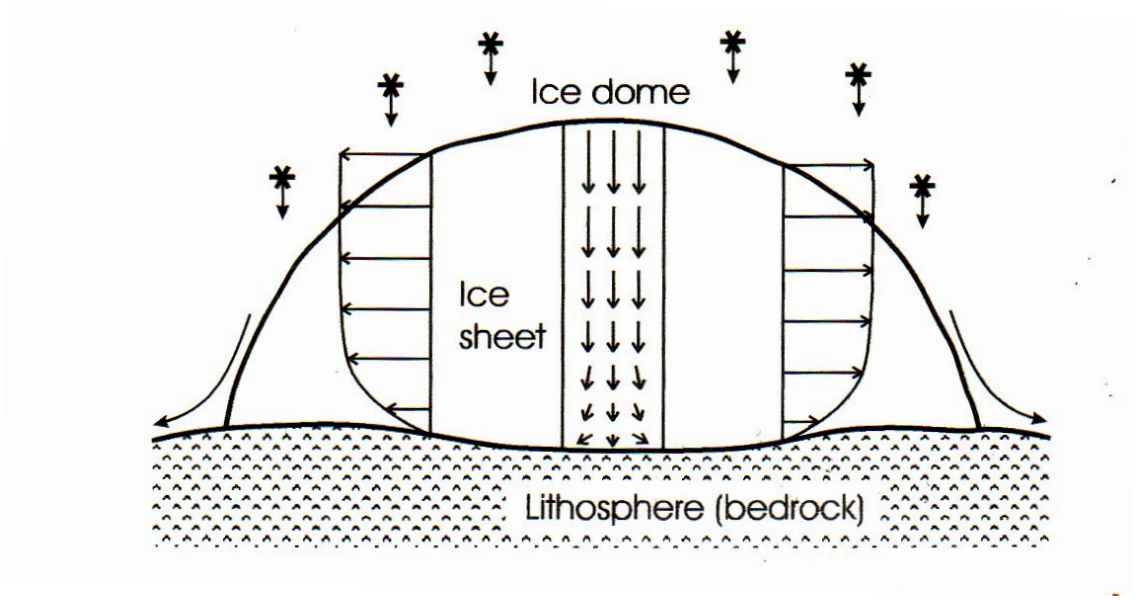

Fig. 2.2: Flow regimes in an ice sheet [Greve., 2004 / 2005].

2.3 Ice-thickness evolution

Figure 2.3 is a schematic picture showing a vertical cross section of an ice sheet. Using kinetic boundary conditions at the surface ($z = h$) and the base ($z = b$),

$$v_z(h) = \frac{\partial h}{\partial t} + \boldsymbol{v}_{hor}(h) \cdot \nabla h - M_s, \tag{12a}$$

$$v_z(b) = \frac{\partial b}{\partial t} + \boldsymbol{v}_{hor}(b) \cdot \nabla b - M_b, \tag{12b}$$

where h is the surface elevation, H the ice thickness, M_s the mass balance at the surface, and M_b the mass balance at the base. The continuity equation (1) is integrated along the vertical axis. This yields

$$\frac{\partial H}{\partial t} = \frac{\partial (h-b)}{\partial t} = -\nabla \cdot \int_b^h dz \boldsymbol{v}_{hor} + M_s + M_b, \tag{13}$$

which means that the local ice thickness is in balance with the divergence of the ice flux and the net input of mass at the surface and the base. The surface mass balance M_s is a climatic boundary condition, whereas the basal mass balance M_b results from the energy jump condition at the base.

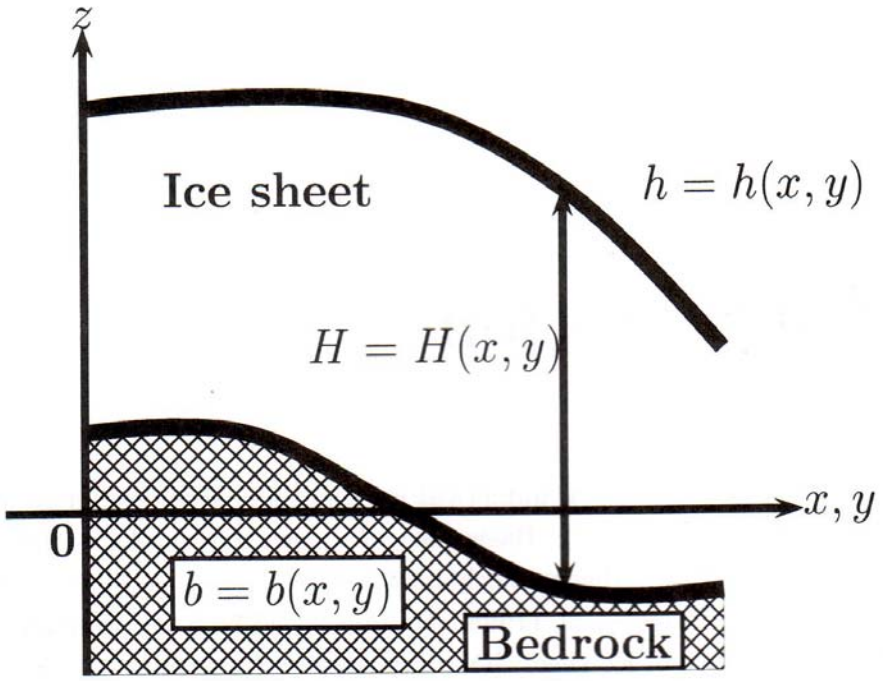

Fig. 2.3: Schematic picture of a vertical cross section of an ice sheet [Saito, 2002].

2.4 Basal sliding

Ice sheets flow not only within the bulk volume by viscous ice deformation, but also at the bed by various basal flow processes. Especially when the bed is melting, basal flow takes an important role in ice sheet dynamics. The basal flow mechanism is considered to be dependent on the subglacial environment. When an ice sheet is underlain by hard rock, melt water reduces the friction between the ice sole and the bedrock, and it enhances the basal sliding. On the other hand, sediment deformation takes place underneath a glacier when an unconsolidated subglacial sediment layer exists.

One of pioneering theoretical works on the basal flow of a glacier on hard rock is Weertman's theory of basal sliding (Weertman., 1957). This theory explains how ice, assumed to be at the melting temperature, moves past bumps in the glacier bed. According to Weertman, ice moves past bedrock bumps by a combination of regelation and enhanced plastic flow.

Till is a complex material and its deformation rate depends not only on the applied shear stress but also on effective pressure, porosity, volume fraction of fines, and strain history. In the present discussion, the till is assumed to be water-saturated, ice free, and isotopic. Only steady-state deformation in simple shear is considered and the strain rate is assumed to depend only on shear stress and effective pressure.

It is reasonable to assume that the ice is frozen to the ground if the basal temperature T_b is below the pressure melting point T_m, so that no-slip conditions prevail. By contrast, if the basal temperature is at pressure melting, basal sliding can be expected, and its amount can be related to the basal shear stress τ_b and the basal overburden pressure p_b in the form of a power law (Weetman-type sliding law). Therefore, the basal-sliding velocity v_b can be expressed as

$$v_b = 0 \qquad \text{if } T_b < T_m, \tag{14a}$$

$$v_b = C_b \frac{\tau_b^p}{p_b^q} \qquad \text{if } T_b = T_m, \tag{14b}$$

where p and q are the basal-sliding exponents, which have been proposed. Suitable choices for their values are (p, q) = (3, 2) for sliding on hard rock, and (p, q) = (1, 0) for sliding on soft, deformable sediment (Greve., 2004 / 2005).

2.5 Temperature field

The energy balance equation (3) is expressed in an Euler form, assuming constant heat capacity and a constant thermal conductivity,

$$\frac{\partial T}{\partial t} = \frac{k_I}{\rho_I c} \nabla \cdot \nabla T - (\boldsymbol{v} \cdot \nabla) T + \frac{\Phi}{\rho_I c}, \tag{15}$$

where the evolution of the internal temperature field is balanced by diffusion, advection and strain heating.

The surface boundary condition for Eq. (15) is provided by prescribing the surface temperature T_s,

$$T = T_s. \tag{16}$$

The basal boundary condition is expressed in two forms. For a cold base, that is, a basal temperature below pressure melting, there can not be any basal melting, and no-slip conditions prevail. Thus,

$$k_I (\mathrm{grad} T \cdot \boldsymbol{n}) = q_{geo}^{\perp}, \tag{17}$$

where $\boldsymbol{n}$ is the normal unit vector of the base and $q_{geo}^{\perp}$ the geothermal heat flux which must be prescribed. By contrast, in case of a temperate base (basal temperature at the pressure melting point), the basal temperature is known, namely

$$T = T_m. \tag{18}$$

3 Experimental design ~ Background of ISMIP HEINO

Calov et al. (2002) demonstrated for the first time that large scale instabilities of the Laurentide Ice Sheet resembling HEs in periodicity, amplitude and spatial extent can be simulated with a 3-D dynamic / thermodynamic ice-sheet model (SICOPOLIS) coupled to an Earth system model (CLIMBER-2). In order to further investigate the dependence of these instabilities on atmospheric and basal conditions and compare the results of different ice-sheet models, the ISMIP HEINO [Ice Sheet Model Intercomparison – Heinrich Event INtercOmparison; see Calov and Greve (2005) and http://www.pik-potsdam.de/ ~calov/heino.html] experiments have been designed.

3.1 3D ice sheet model SICOPOLIS

The model SICOPOLIS (Simulation Code for POLythermal Ice Sheet) simulates the large-scale dynamics and thermodynamics (ice extent, thickness, velocity, temperature, water content and age) of ice sheets three-dimensionally and as a function of time (Greve., 1997). In the case of ISMIP HEINO, ice sheet is a main component of the model, and atmospheric (accumulation, ablation, and temperature) and lithospheric variables (geothermal heat flux) are used for inputs (Fig. 3.1).

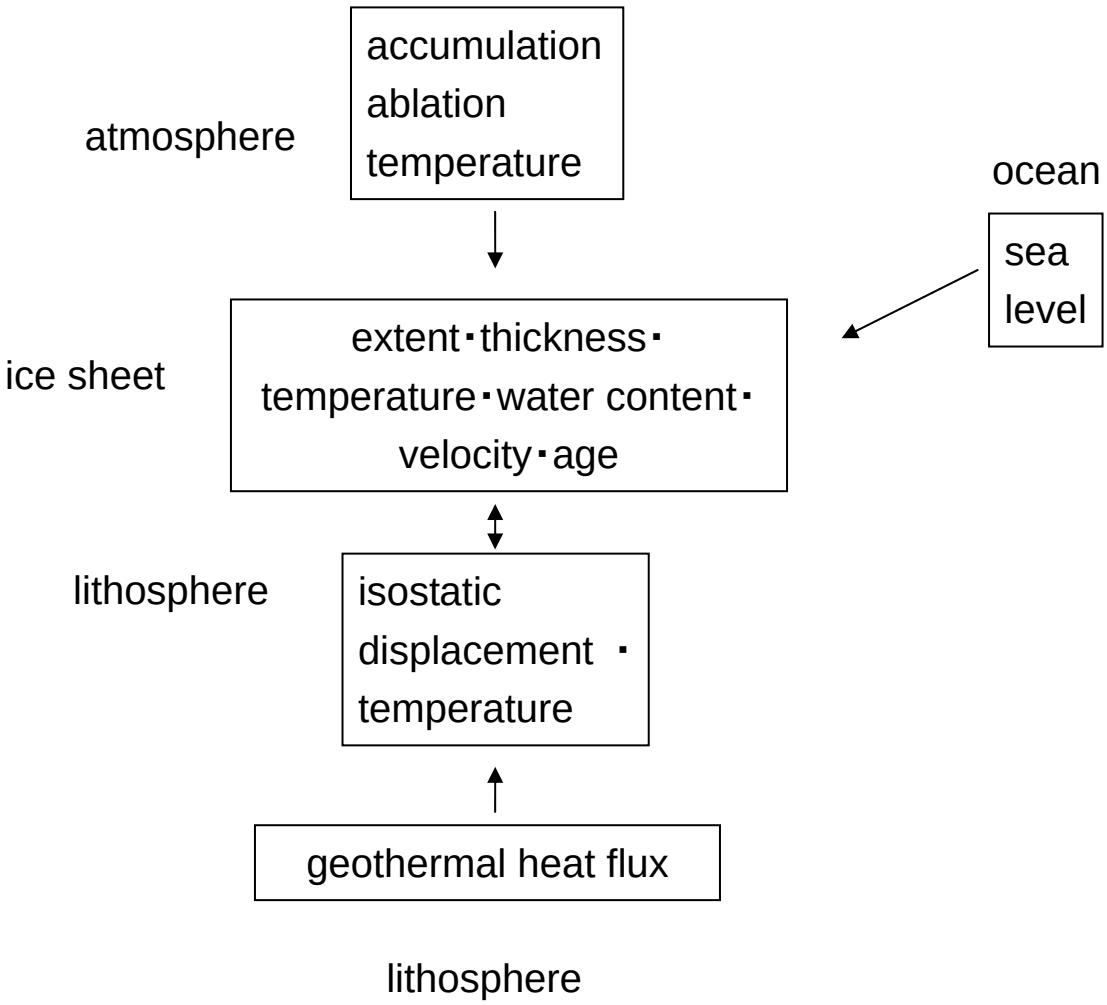

Fig. 3.1: 3D ice sheet model SICOPOLIS (Greve., 1997)

3.2 Model domain

The model domain is a flat horizontal square of the size 4000×4000 km,

$$x = 0\ldots4000 \text{ km}, \quad y = 0\ldots4000 \text{ km} \tag{19}$$

discretized by a 50-km grid, where x, y are the horizontal Cartesian coordinates. This leads to 81×81 grid points indexed by

$$i = 1...81, \quad j = 1...81 \text{ (for SICOPOLIS)}. \tag{20}$$

The land area which is prone to be glaciated is situated within the circle

$$d = \sqrt{\left(x - \hat{x}\right)^2 + \left(y - \hat{y}\right)^2} < R, \tag{21}$$

where the center of the domain has the position

$$\left(\hat{x}, \hat{y}\right) = (2000km, \quad 2000km). \tag{22}$$

d denotes the distance from the center, and the radius is R = 2000 km. The area outside the circle is assumed to be ocean, where the ice thickness always equals zero.

Within the land area defined by Eq. (21) two different types of bedrock are distinguished: (i) hard rock, and (ii) soft sediment. Soft sediment is assumed for the region of "Hudson Bay" within the square (including the borders) defined by the points

A = (2300 km, 2500 km), C = (3300 km, 2500 km),

B = (2300 km, 1500 km), D = (3300 km, 1500 km),

and "Hudson Strait" within the rectangle (including the borders)

E = (3300 km, 2100 km), G = (4000 km, 2100 km),

F = (3300 km, 1900 km), H = (4000 km, 1900 km).

For the remaining part of the model domain, hard rock is assumed (Fig. 3.2).

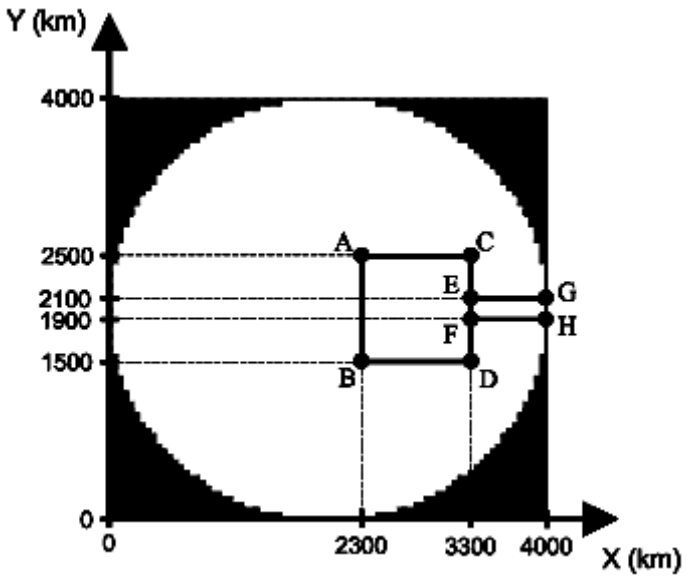

Fig. 3.2: HEINO model domain. The land area is shown in white, the ocean is black. The area inside the square ABDC ("Hudson Bay") and the rectangle EFHG ("Hudson Strait") correspond to the soft sediment bed. The remaining area is hard rock.

3.3 Boundary conditions setting

3.3.1 Surface condition

The surface accumulation b is assumed to increase linearly from the value at the center b_{min} = 0.15 m ice equiv. a^{-1} over the radius R = 2000 km to the value at the margin b_{max} = 0.3 m ice equiv. a^{-1}, that is

$$b = b_{min} + \frac{b_{max} - b_{min}}{R} \times d \,. \tag{23}$$

Surface ablation is not considered. However, it is assumed that the coastward ice-mass flux is discharged into the surrounding ocean when it crosses the margin, where the ice thickness is zero. The surface mass balance M_s (sect. 2.3) is therefore equal to the accumulation b.

The surface temperature T_s is assumed to increase with the third power of the distance d from the center of the model domain towards the margin,

$$T_s = T_{min} + S_T d^3 , \tag{24}$$

with the surface temperature at the center T_{min} = 233.15 K and the horizontal gradient S_T= 2.5×10^{-9} K km^{-3}.

A sketch of surface condition settings is shown in Figure 3.3.

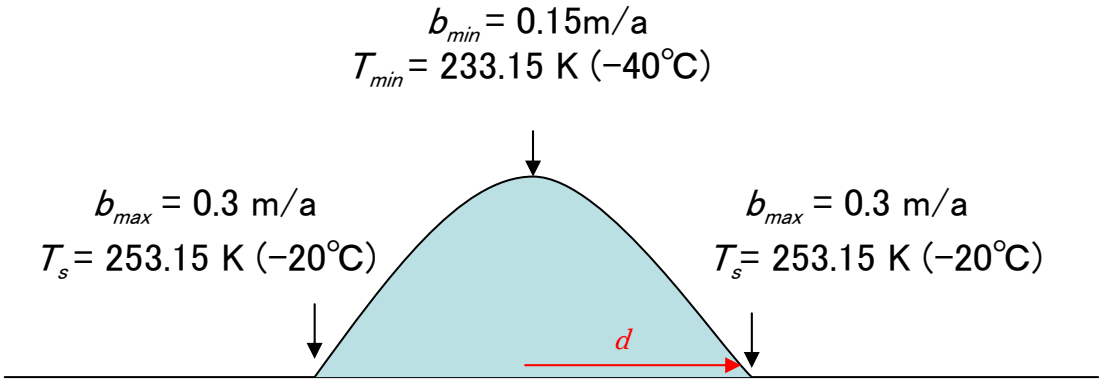

Fig. 3.3: Sketch of the surface accumulation and temperature at the center and the margin of the model domain. The surface accumulation b increases linearly from the center to the margin. The surface temperature T_s increases with the third power of the distance d from the center of the domain towards the margin.

3.3.2 Basal condition

The basal velocity was introduced from Eq. (14) in chapter 2 as

$$v_b = 0 \qquad \text{if } T_b < T_m, \tag{25a}$$

$$v_b = C_b \frac{\tau_b^p}{p_b^q} \qquad \text{if } T_b = T_m, \tag{25b}$$

where the basal shear stress τ_b and the basal overburden pressure p_b are given as

$$\tau_b = \rho g H \nabla h, \tag{26}$$

$$p_b = \rho g H. \tag{27}$$

We substitute (26) and (27) into (25b) and replace the sliding parameter C_b into C_R if the bed is hard rock, or C_s if the bed is covered by soft sediment. Therefore Eqs. (25b) become

$$v_b = -C_R H \left|\nabla_H h\right|^2 \nabla_H h \quad \text{for } T_b = T_{pmp} \text{ and hard rock,} \tag{28a}$$

$$v_b = -C_S H \nabla_H h \quad \text{for } T_b = T_{pmp} \text{ and soft sediment,} \tag{28b}$$

$$v_b = 0 \quad \text{for } T_b < T_{pmp,} \tag{28c}$$

where $\nabla_H = (\partial/\partial x, \partial/\partial y)$ is the horizontal gradient, T_b the basal temperature and T_{pmp} the pressure-melting point of ice. The sliding parameters for hard rock and soft sediment are $C_R = 10^5$ a^{-1} and $C_S = 500$ a^{-1}, respectively.

In order to estimate the order of magnitude of the basal sliding, we assume a large ice sheet with a maximum thickness of about 3 km (H = 3 km), a gradient of the surface toward the x coordinate of 0.2 degrees and no surface slope toward the y coordinate. This yields ($\frac{\partial h}{\partial x} = 3.5 \times 10^{-3}$, $\frac{\partial h}{\partial y} = 0$). The basal temperature is at the pressure melting point. Under these assumptions, the basal velocity v_{bx} is 12.8 m/yr if the base is hard rock, whereas the basal velocity is 5.25 km/yr if the base is covered by soft sediment. Of course, the basal velocity is zero if the basal temperature is below pressure melting.

Therefore, the order of the basal velocity on subglacial soft sediment is about hundred times larger than the one on hard rock.

3.4 Further settings

The ice sheet is built up from zero ice thickness over 200 kyr, with a temporally constant glacial-climate forcing as described above. The bedrock elevation remains constant (flat) throughout the simulations (no isostasy), and the geothermal heat flux is applied directly at the bottom of the ice sheet (no thermal bedrock). For the 50-km grid spacing, we used a common time step of 0.25 years for both the evolutions of topography and temperature.

The HEINO standard run (ST) is defined by the setting given in Section 3.3 and the parameters listed in Table 3.1.

Parameter	**Value**
Density of ice, ρ	910 kgm^{-3}
Gravity acceleration, g	9.81 ms^{-2}
Power-law exponent, n	3
Flow-enhancement factor, E	3
Sliding parameter for hard rock, C_R	10^5 a^{-1}
Sliding parameter for soft sediment, C_S	500 a^{-1}
Geothermal heat flux, q_{geo}	4.2×10^{-2} Wm^{-2}
Melting temperature of water, T_0	273.15 K
Heat conductivity of ice, κ	2.1 $Wm^{-1}K^{-1}$
Specific heat of ice, c	2009 $Jkg^{-1}K^{-1}$
Clausius-Clapeyron gradient, β	8.7×10^{-4} Km^{-1}
Latent heat of ice, L	3.35×10^5 Jkg^{-1}
Universal gas constant, R	8.314 $Jmol^{-1}K^{-1}$
Seconds per year	31556926 sa^{-1}

Table. 3.1: Values of the physical parameters used for HEINO.

3.5 Standard model run (ST)

With the above settings, we carry out the standard run (ST). We look into the details of the result of ST in terms of 1) global time series, 2) time series over the sediment region, and 3) time series at certain grid points.

3.5.1 Global time series

We tried to get global time series consisting of the ice volume and temperate basal area for the whole ice sheet.

3.5.2 Time series over the sediment region

Here, we are interested in the sediment region only. For this region, we studied the average ice thickness, the average homologous basal temperature and the maximum surface velocity during the last 50 ka.

3.5.3 Time series at certain grid points

Seven grid points over the sediment region are defined as follows,

P_1 = (3900 km, 2000 km), P_5 = (3200 km, 2000 km)
P_2 = (3800 km, 2000 km), P_6 = (2900 km, 2000 km)
P_3 = (3700 km, 2000 km), P_7 = (2600 km, 2000 km)
P_4 = (3500 km, 2000 km),

and are displayed in Figure 3.4.

We tried to get time-series output of the ice thickness, homologous temperature and basal frictional heating.

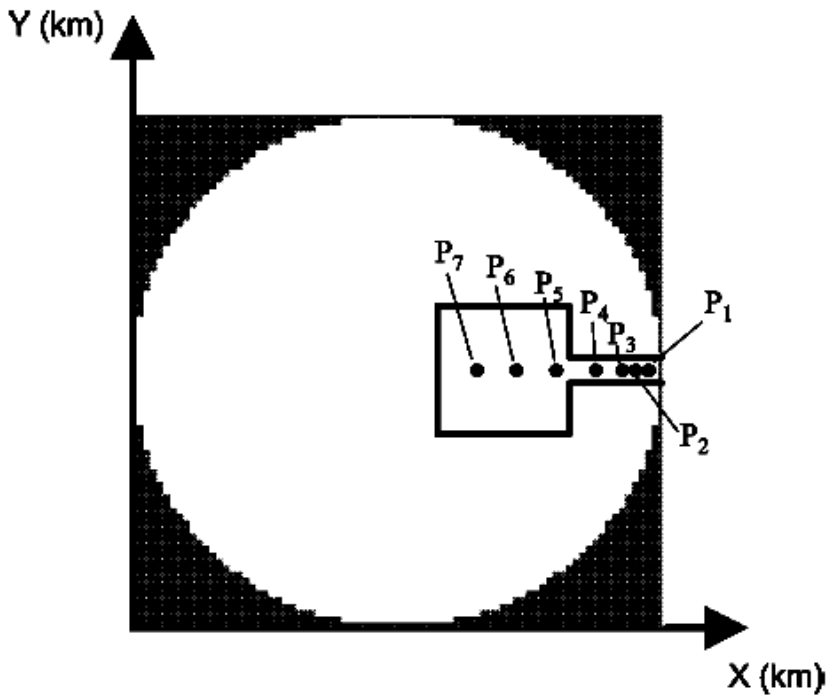

Fig. 3.4: Positions on the grid in the sediment region where time series output is required.

3.6 Parameter studies

In order to investigate the influence of boundary conditions on the modeling results, parameter studies were performed.

3.6.1 Variation of the surface boundary conditions

The minimum temperature T_{min} in equation (24) (section. 3.3.1) is varied by ±10 K, resulting in the setting T_{min} = 223.15 K for run **T1** and T_{min} = 243.15 K for run **T2**.

The surface accumulation in equation (23) (section. 3.3.1) is changed by a factor of 0.5 and 2. The corresponding parameter values are b_{min} = 0.075 m ice equiv. a^{-1}, b_{max} = 0.15 m ice equiv. a^{-1} for run **B1**, and b_{min} = 0.3 m ice equiv. a^{-1}, b_{max} = 0.6 m ice equiv. a^{-1} for run **B2**.

3.6.2 Variation of the sediment-sliding parameter

The sediment-sliding parameter C_s is varied as C_s = 100 a^{-1} (run **S1**), C_s = 200 a^{-1} (run **S2**) and C_s = 1000 a^{-1} (run **S3**).

3.6.3 Variation of the time step

Time step for both of the evolutions of topography and temperature is set at 0.5 years (ST-05), 1 year (ST-1), and 2 years (ST-2), respectively.

3.7 Rotated grid tests

In order to investigate whether the result of the standard run ST is influenced by the alignment of the numerical grid (parallel to the x and y directions) to the sediment area (which represents Hudson Bay and Hudson Strait), the standard run ST has been re-run 9 times, with a sediment area rotated by 5° (STr-05), 10° (STr-10), 15° (STr-15), 20° (STr-20) 25° (STr-25) 30° (STr-30) 35° (STr-35), 40° (STr-40) and 45° (STr-45), respectively, around the center of the model domain. The rotation by 45° is shown in Figure 3.5 (see Fig. 3.2 for comparison).

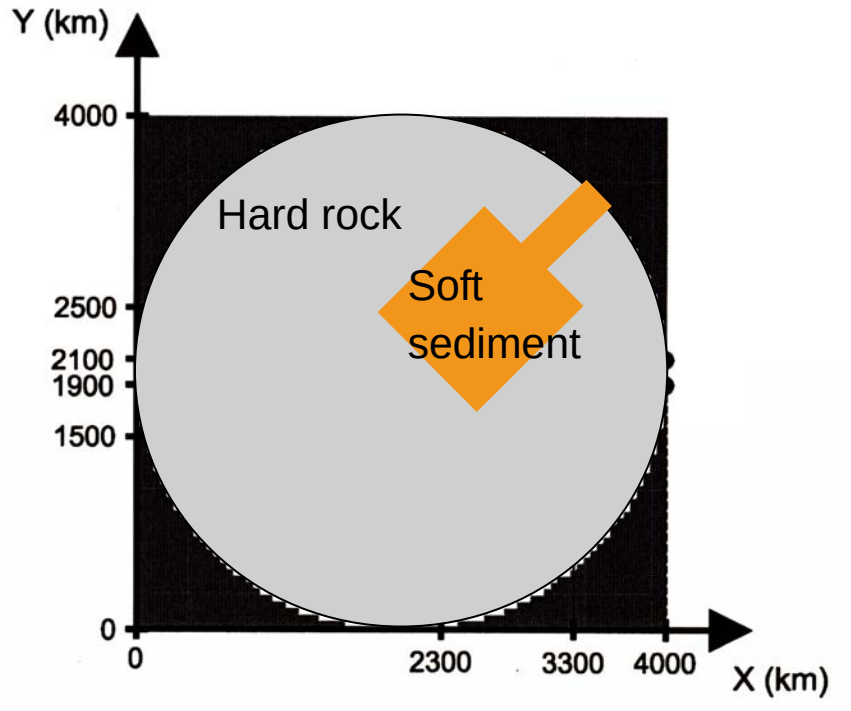

Fig. 3.5: Rotated domain of ISMIP HEINO. The sediment area mimics Hudson Bay (square) and Hudson Strait (channel towards top right).

4 Results and discussions

4.1 Results of the standard model run

4.1.1 Results of global time series

Figure 4.1 shows total ice volume variation over the model time from 0 to 200 kyr. Saw-shape oscillations indicate series of growing ice sheet and HE. The growing time is about 7 ka, whereas the subsequent HE collapse lasts only some hundred years. The average of ice volume is about 36 $\times$ 10^6 km^3.

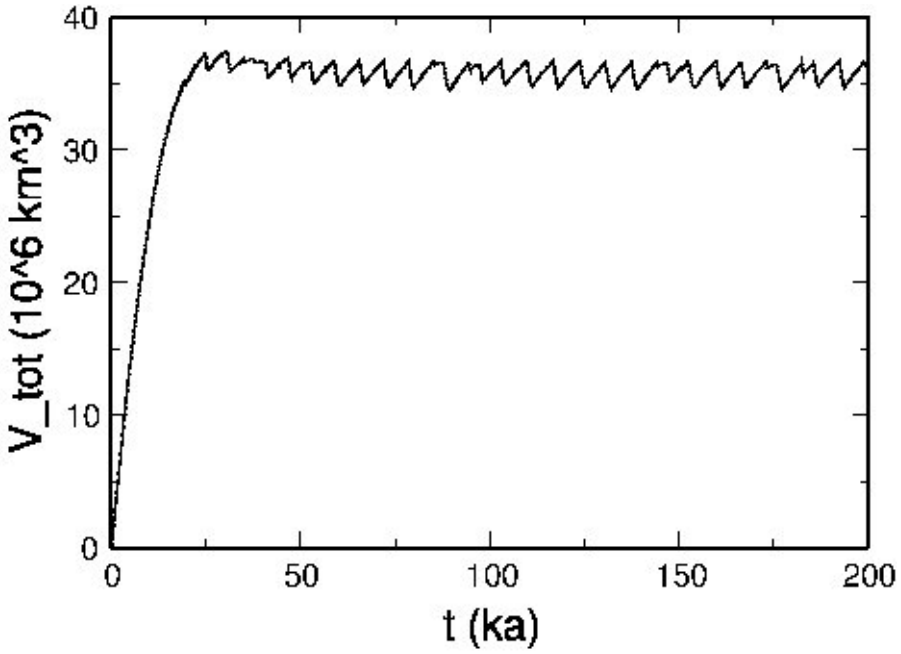

Fig. 4.1: Total ice volume variation over the model time from 0 to 200kyr.

4.1.2 Results of time series over the sediment region

Figure 4.2 shows the evolution of the ice sheet during the last 50 kyr. Figure 4.2 (a) shows the mean thickness H_{ave} over the sediment region. The average basal temperature relative to pressure melting point, $T'_{b,\ ave}$ over the sediment region is shown in Figure 4.2 (b). Figure 4.2 (c) shows the maximum average surface velocity $v_{s,\ ave}$ over the land area. According to the ISMIP HEINO description (Calov and Greve., 2005) the times t_1 ~ t_4 are defined as the times of maximum (t_1) and minimum (t_2) average ice thickness, minimum average basal temperature (t_3) and maximum basal area at pressure melting (t_4) for the sediment area during the last 50 ka. These are indicated in Figure 4.2.

Figure 4.3 shows two dimensional plots of variables at each time phase of a HE. Ice thickness, basal homologous temperature, and surface velocity before a HE (t_1) are shown in Figure 4.3 (a), (b), and (c), respectively. Similarly, (e) and (f) are basal homologous temperature and surface velocity during a HE (t_4), respectively. Ice thickness after a HE (t_4) is shown in (d).

We can see that the maximum ice thickness is about 4.1 km, and the minimum is about 3.1 km. Accordingly, the amplitude of the ice thickness variation is about 1 km (Fig. 4.2 (a)). Each full cycle consists of a gradual growth phase, followed by a massive surge (HE).

During the growth phase, homologous basal temperatures are below the pressure melting point for most of the sediment region (Fig. 4.2 (b), Fig. 4.3 (b)), and ice flows slowly by internal deformation only (Fig. 4.2 (c), Fig. 4.3 (c)). As the ice gets thicker enough because of snowfall, thermal insulation against the cold surface increases. Then, the basal temperature rises gradually, until the pressure melting point is reached at the mouth of Hudson strait. At that time, rapid basal sliding starts and leads to increased strain heating. As a consequence, an "activation wave" develops, which travels upstream very quickly (about a hundred years) until almost the

entire sediment area is at pressure melting. This wave represents a rapid upstream migration of a sheep gradient of the ice sheet elevation. The steep gradient itself produces an intensified ice flow adjacent to the front and causes a large increase of dissipation of mechanical energy, which warms the bottom of the ice sheet to the pressure melting point. As a result, the temperate basal area spreads upstream.

During the surge phase, the ice flow velocity reaches values up to 8 km a^{-1} (Fig. 4.2 (c), Fig. 4.3 (f)), and the ice sheet collapses rapidly. During the surge, the ice sheet becomes thinner and its surface slope towards Hudson Strait decreases. Eventually, the rate of energy dissipation becomes insufficient to sustain melting at the base and the basal temperature rapidly drops below the melting point. This causes a rapid retreat of the temperate basal area downstream ("deactivation wave"). Then the surge stops, and the next growth phase begins.

In addition to the main oscillation, the signal of the maximum surface velocity (Fig. 4.3 (c)) shows a number of additional, higher frequency peaks, which are only slightly observed in the signals of the ice thickness and the basal temperature. These peaks are caused by small scale sediment sliding at the mouth of Hudson Strait, because the increased strain heating is not strong enough to initiate an 'activation wave'. Two dimensional distributions of ice thickness, and surface velocity during a 'mini-HE', which continues for less than two hundred years, are compared with those of a HE in Figure 4.4.

In the 'mini-HE', the fast ice flow is limited at Hudson strait (see (d) and (e)), and the collapse of the ice sheet can be seen only at Hudson strait (see (a) - (c)). On the other hand, the expansion of the fast ice flow can be seen at the part of Hudson Bay and whole Hudson strait (see (j) and (k)), and the collapse of the ice sheet reached at Hudson Bay during the HE (see (g) - (i)).

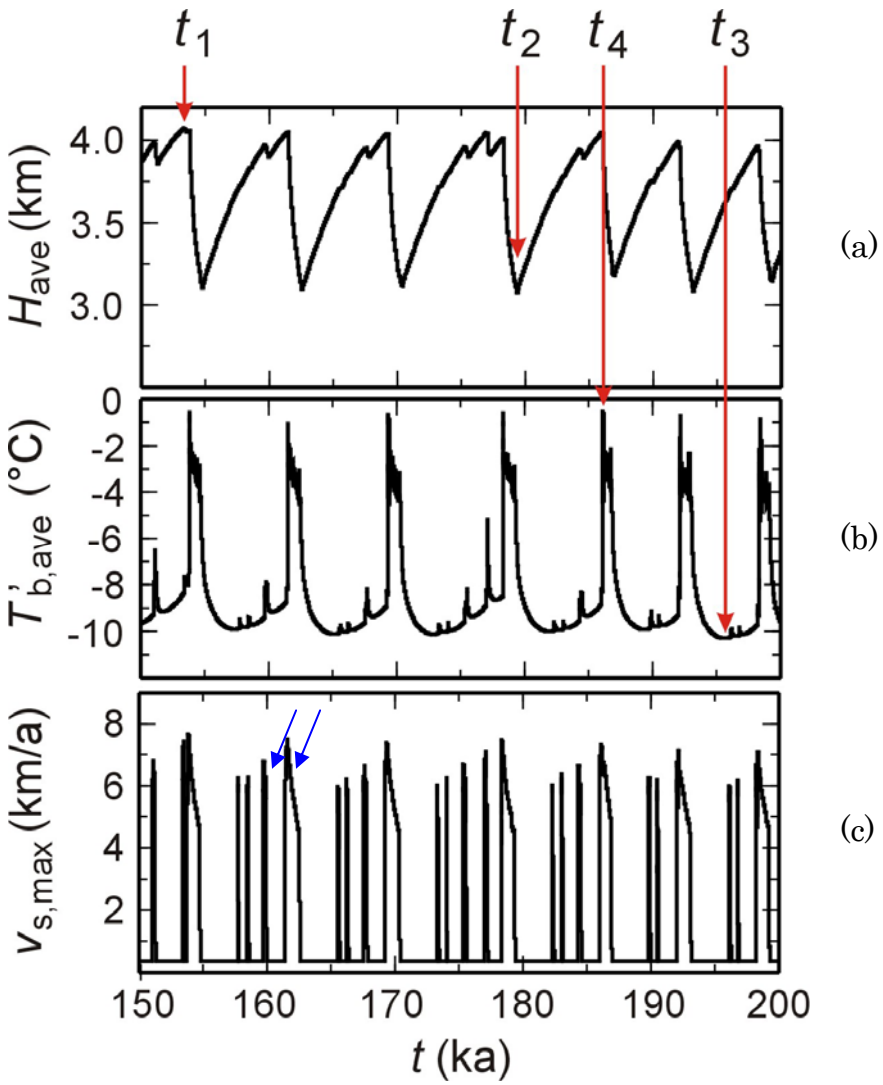

Fig. 4.2: Top panel: Average thickness H_{ave} over the sediment region. Middle panel: Average homologous basal temperature $T'_{b,\,ave}$ over the sediment region. Bottom panel: Maximum surface velocity $v_{s,max}$ over the sediment region. The times t_1 ~ t_4 are defined as the times of the maximum (t_1) and the minimum (t_2) average ice thickness, the minimum average basal temperature (t_3) and the maximum basal area at pressure melting (t_4) for the sediment area during the last 50 kyr. The peaks of a typical mini HE and a typical HE are indicated by blue arrows in the bottom panel.

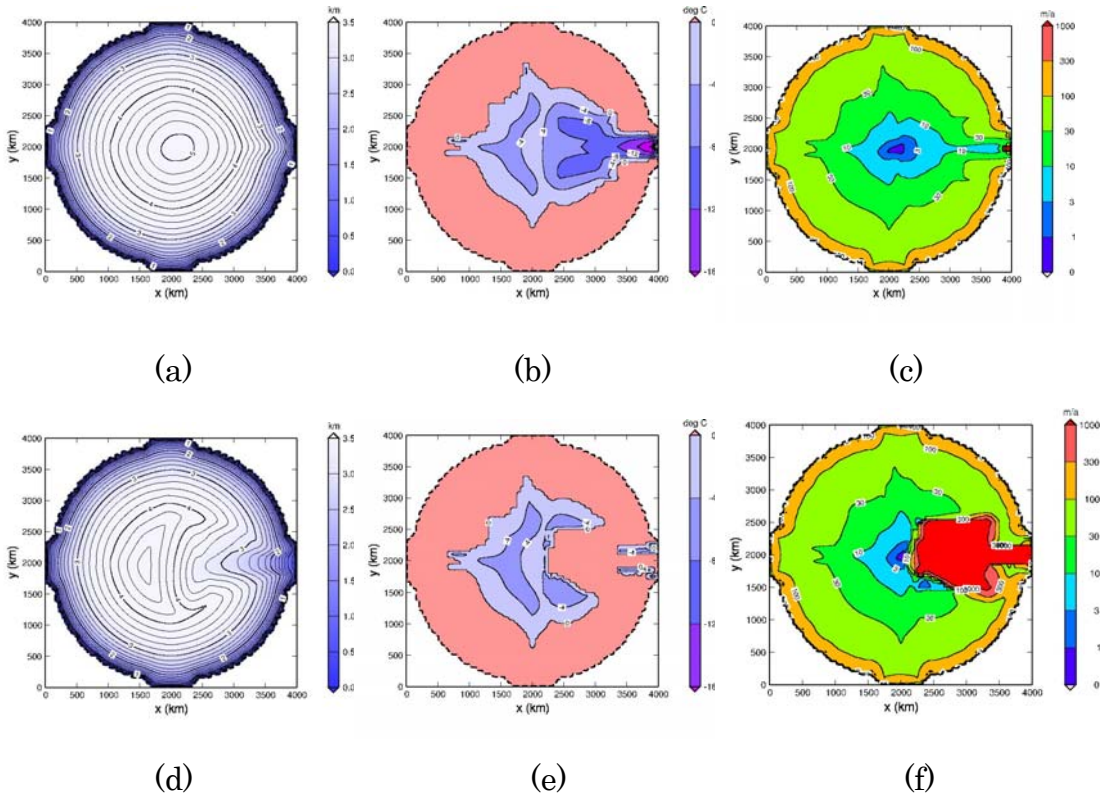

Fig. 4.3: (a) Ice thickness, (b) basal temperature relative to the pressure melting point, and (c) surface velocity before a HE (t_1). (d) Ice thickness after a HE (t_2). (e) Basal temperature relative to pressure melting point, and (f) surface velocity during a HE (t_4).

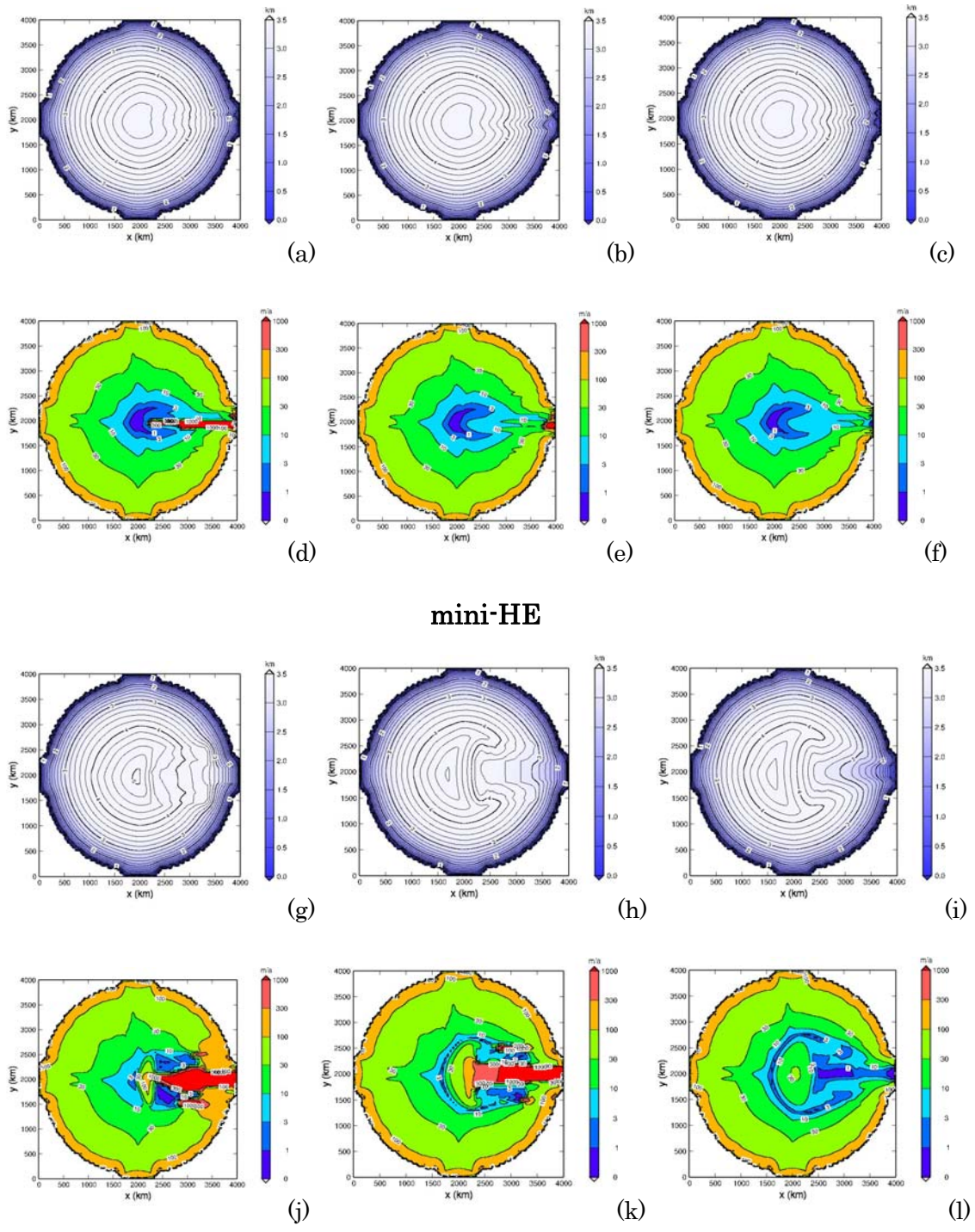

Fig. 4.4: Temporal evolution of ice thickness and surface velocity distributions during a mini HE (a)-(f) and a HE (g)-(l). Panels of (a), (d), (g), and (j): When a mini HE or a HE starts. Panels of (b), (e), (h), and (k): During a mini HE or a HE. Panels of (c), (f), (i), and (l): When a mini HE or a HE finishes.

4.1.3 Results of time series for certain grid points

Evolutions of mean ice thickness over the sediment area at certain points (P1 ~ P7) during the last 50 kyr are shown in Figure 4.5.

There are two important characteristic features in Figure 4.5. First, the interval of the oscillations of the ice thickness at sediment grid points P1 ~ P7 increases with the distance from the ice margin: the intervals of ice thickness oscillation at P1 vary from 2.5 kyr to 4 kyr, whereas they vary from 6 kyr to 10 kyr at P7.

Second, small perturbations which can be seen at P1 are gradually bound to form larger perturbations which can be seen at P7.

These observations suggest that each of the second or third instability (mini-HEs) at the mouth of Hudson Strait triggers the large-scale instability (HEs) over Hudson Bay and Hudson Strait.

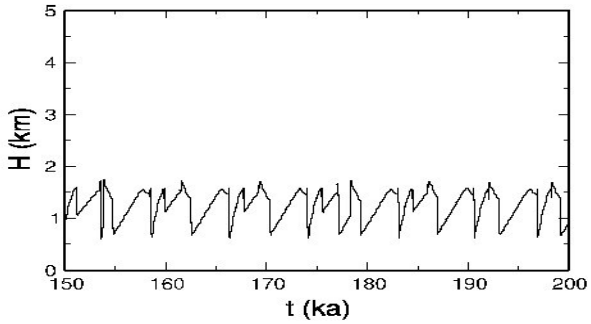
H (km)
t (ka)
0
1
2
3
4
5
150
160
170
180
190
200

P1

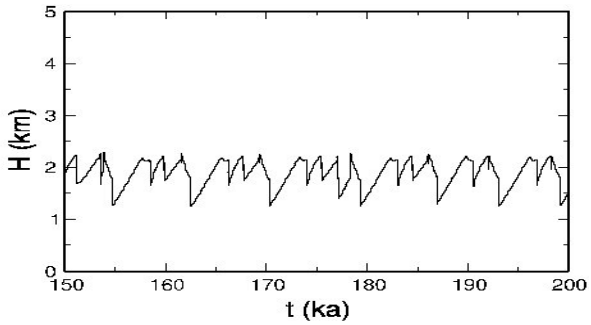
H (km)
t (ka)
0
1
2
3
4
5
150
160
170
180
190
200

P2

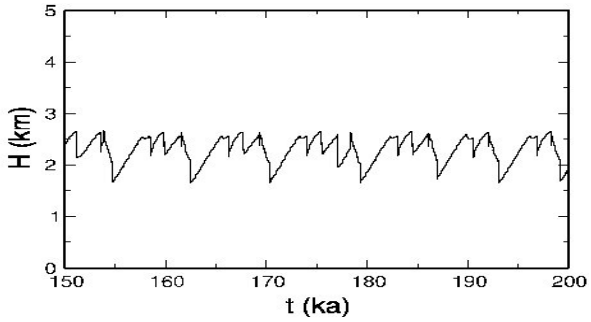
H (km)
t (ka)
0
1
2
3
4
5
150
160
170
180
190
200

P3

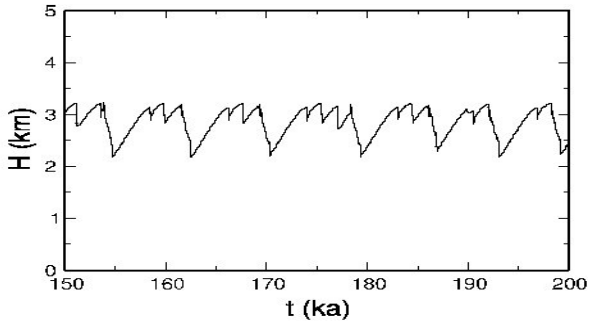
H (km)
t (ka)
0
1
2
3
4
5
150
160
170
180
190
200

P4

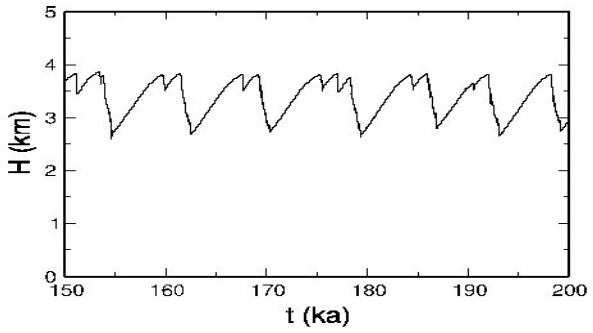

P5

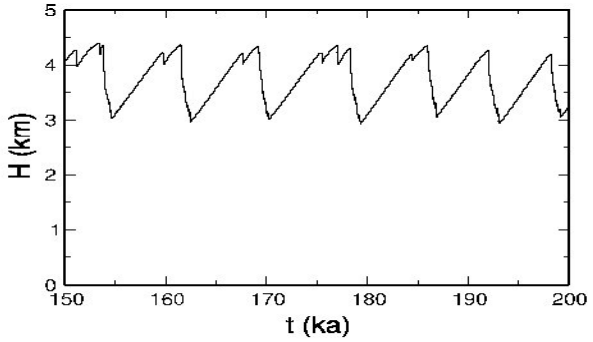

P6

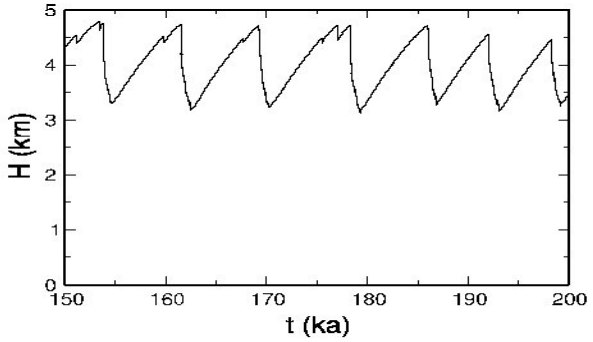

P7

Fig. 4.5: Time series of the ice surface elevation at certain grid points (P1 ~ P7) over the sediment region (Fig. 3.4) in run ST.

4.2 Results of parameter studies

4.2.1 Result of variation of the surface conditions

Evolutions of mean ice thickness over the sediment area with changed surface boundary conditions during the last 50 kyr and the power spectrum of each evolution are shown in Figure 4.6. The top panels (a) and (b) are results obtained by using standard surface temperature and accumulation (ST). The second ((c), (d)) and third ((e), (f)) rows are results obtained by using surface-temperature offsets of -10℃ (T1) and +10℃ (T2), respectively. The forth ((g), (h)) and fifth ((i), (j)) rows are results obtained by using half surface accumulation (B1) and twice surface accumulation (B2), respectively.

We can see that the average ice thickness over the sediment region of ST oscillates between approx. 3.1 km to 4.1 km, and the interval of the oscillation is approx. 7500 years ((a), (b)). On the other hand, the ice thickness oscillates from approx. 3.5 km to 4.5 km in T1 (see (c)), and the ice thickness oscillates from approx. 2.5 km to 3.2 km in T2 (see (e)). These results show that the ice sheet grows thicker when the surface temperature is colder, whereas there is little difference in the oscillation intervals. The reason for this behavior is that the surface temperature mainly decides the thickness when a HE occurs. If the surface temperature is colder, the ice sheet needs to grow thicker until it contains sufficient internal heat to melt the base and release a HE.

In contrast to the results above, the interval of ice thickness oscillation of B1 is approx. 15000 years (see (h)), and the period of ice thickness oscillation of B2 is approx. 4500 years (see (i)). These results show that the growth time of the ice sheet until a HE occurs is shorter, if the surface accumulation rate is larger. This is so because the accumulation rate decides the growth time until a HE occurs. If the accumulation rate is larger, the ice sheet grows faster and reaches earlier the threshold thickness which is needed to melt

the base and release a HE.

Therefore, surface temperature affects mainly the ice volume, and surface accumulation affects mainly the periodicity of HEs.

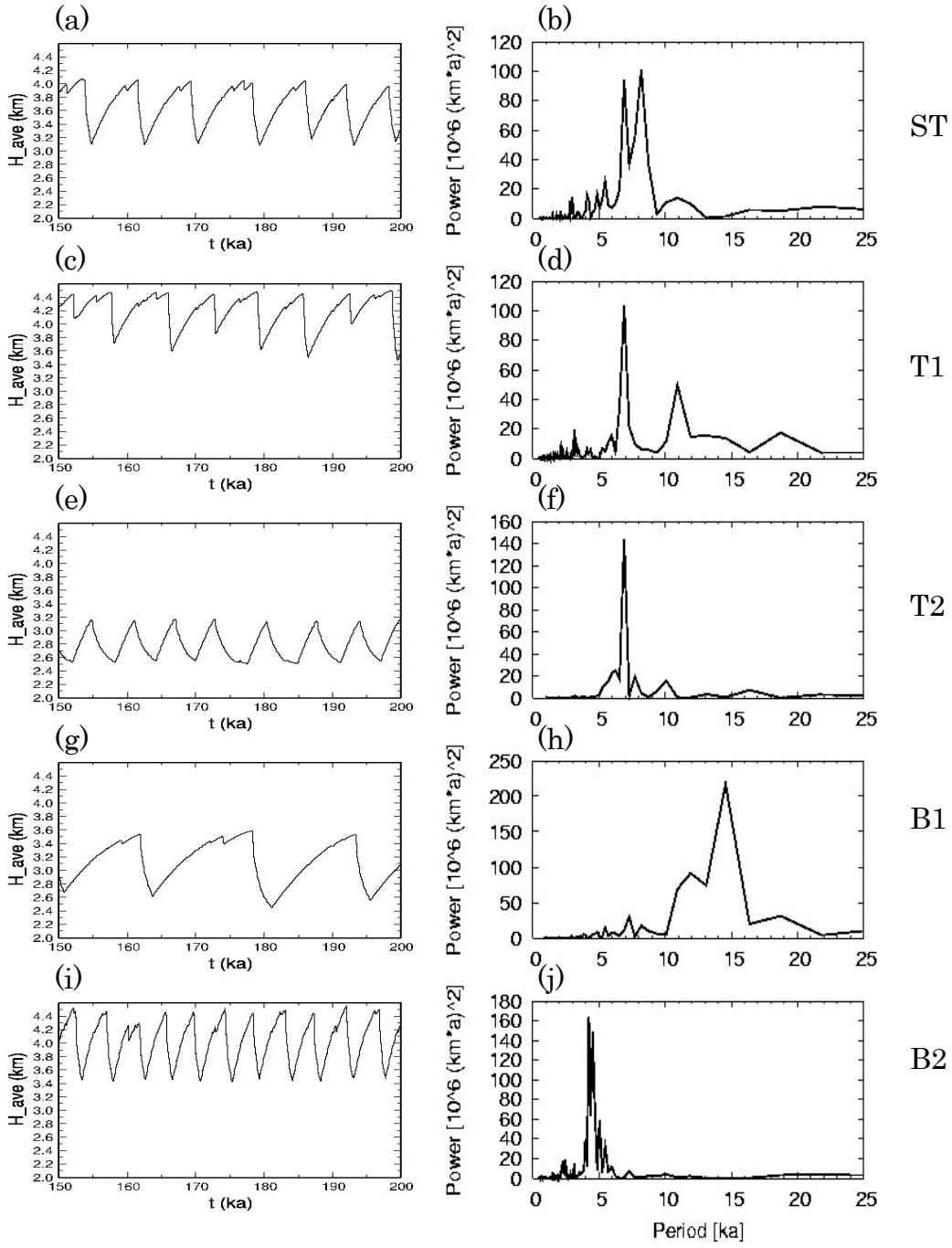

Fig. 4.6: (a) Time series of mean ice thickness, H_{ave}, and (b) the power spectrum for run ST. Similarly, (c) and (d) are for T1, (e) and (f) for T2, (g) and (h) for B1, (i) and (j) for B2, respectively.

4.2.2 Results of variation of the sediment-sliding parameter sediment

The evolutions of mean ice thickness over the sediment area with changed bottom boundary conditions during the last 50 kyr and the power spectra of each evolution obtained by using Fourier transform are shown in Figure 4.7.

The amplitude of ice thickness variation is approx. 0.5 km in S1 (see (a)), 0.6 km in S2 (see (c)), 1 km in ST (see (e)), and 1.4 km in S3 (see (g)), while the interval of the oscillation is nearly independent of the sliding parameter except for S1 (see (b), (d), (f), and (h)).

The amplitude of the oscillations increases as the parameter C_s becomes larger. As the sliding parameter C_s is larger, the subglacial sediment which is at pressure melting deforms more rapidly. So the ice on the sediment flows faster and more ice flows into the ocean. This causes the oscillations to be more pronounced. After a surge, the ice sheet grows to the required thickness at which the next HE can occur.

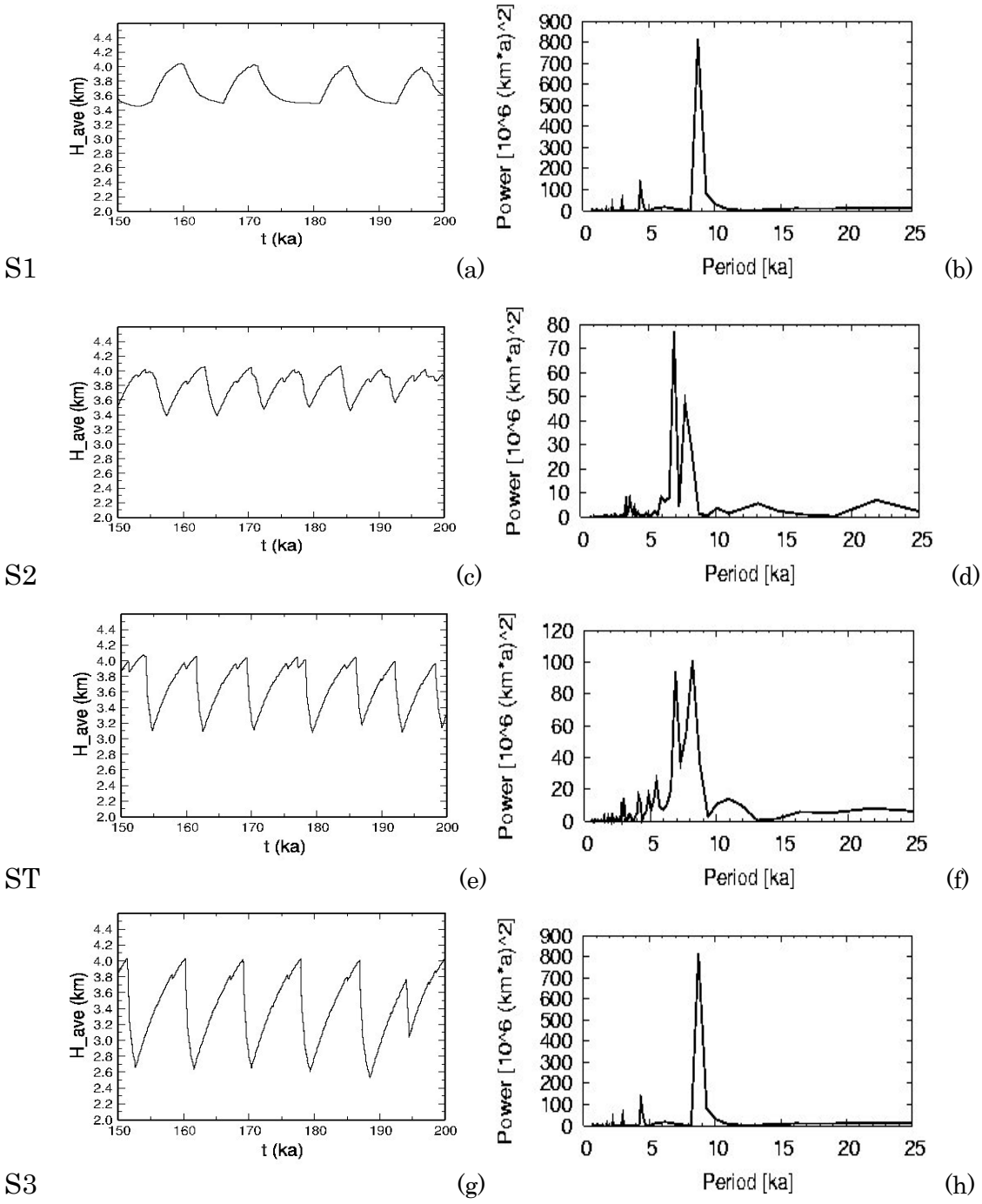

Fig. 4.7: Time series of average ice thickness, H_{ave}, and power spectrum for runs S1 ((a), (b)), S2 ((c), (d)), ST ((e), (f)) and S3 ((g), (h)), where sediment sliding parameters are C_s = 100, 200, 500 and 1000 a^{-1}.

4.2.3 Results of variation of the time step

The evolutions of mean ice thickness over the sediment area with changed time step during the last 50 kyr and the power spectrum for each evolution by using Fourier transform are shown in Figure 4.8. First row ((a), (b)) is result obtained by using the standard time step 0.25 years (ST). The second ((c), (d)) and third ((e), (f)) rows are results obtained by using time steps of 0.5 years (ST - 05) and 1 year (ST - 1), respectively. The bottom row ((g), (h)) is a result obtained by using a time step of 2 years (ST - 2).

The interval of the ice thickness oscillations is different from each other with changed time step. We can see that the amplitude and the period of the ice thickness oscillations converge reasonably well, as the time step is decreased from 2 years to 0.25 years (see Fig. 4.8). However, the fine structure of the ice thickness oscillations does not convergence perfectly. If the time step were chosen even smaller, the convergence would certainly be further improved. However, with time steps of 0.1 years and less the computing time becomes excessive, and therefore a value of 0.25 years can be considered a reasonable compromise.

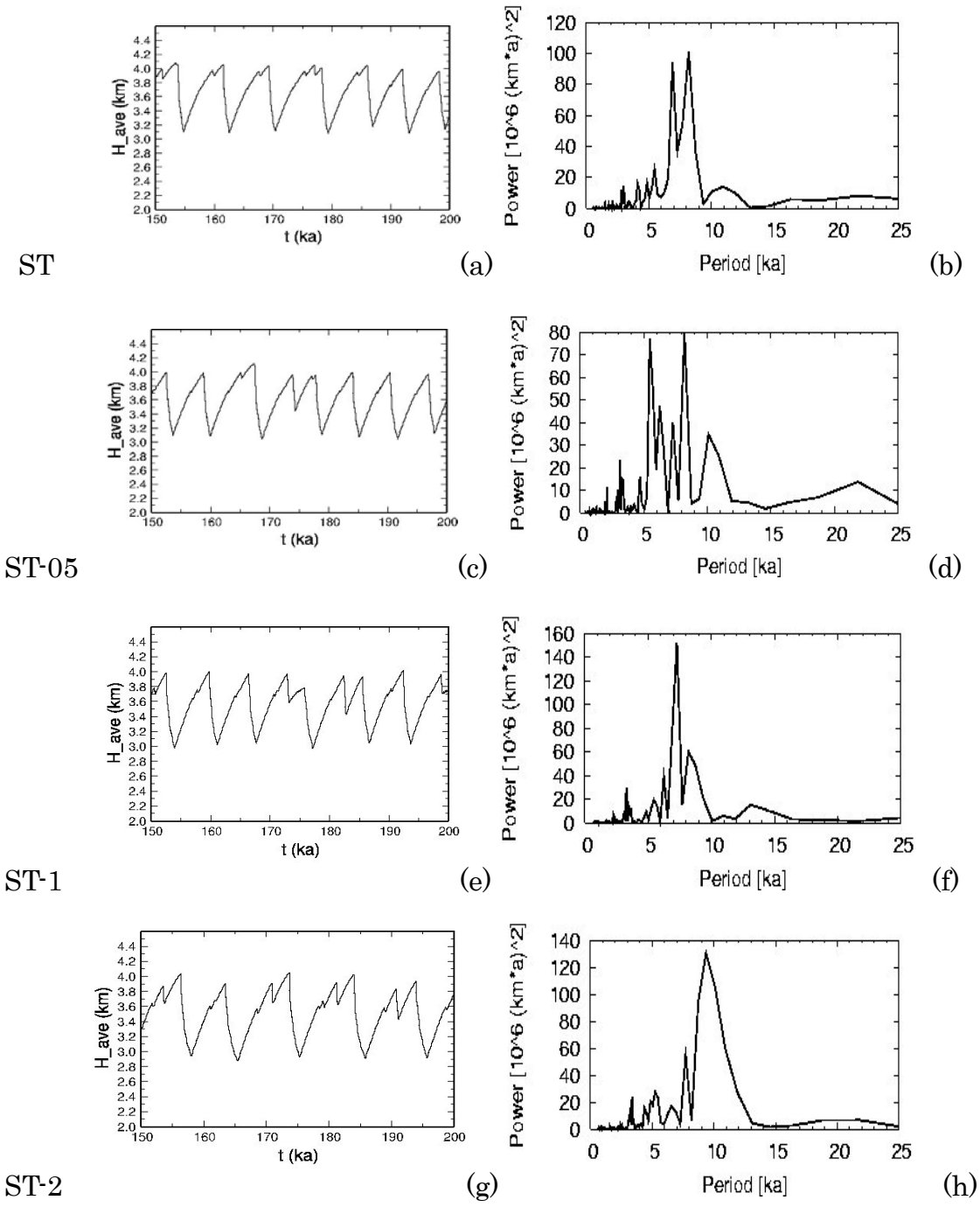

Fig. 4.8: Evolution of averaged ice thickness over the sediment area with changed time step during the last 50 kyr and power spectrum by using Fourier transform. (a) and (b) are for the standard time step 0.25 years (ST), (c) and (d) are for time step 0.5 years (ST-05), (e) and (f) are for time step 1 year (ST-1), and (g) and (h) are for time step 2 years (ST-2).

4.3 Results of rotated grid tests

Nine rotated grid tests (STr-05, STr-10, STr-15, STr-20, STr-25, STr-30, STr-35, STr-40, STr-45) were carried out and compared with ST.

Results of the time series of mean ice thickness H_{ave} over the sediment region during the last 50 kyr and power spectrums of the average ice thickness H_{ave} of each runs by using Fourier transform are shown in Figure 4.9. Evidently, very similar internal ice sheet oscillations (growth-phases followed by large-scale surges) are observed for all tests.

Time series of maximum surface velocity over the land area during the last 50 kyr are shown in Figure 4.10. During the surge, flow velocities of up to 8 km/a are developed. Wider peaks are derived from large-scale surges (HEs), whereas thinner peaks are from small-scale instabilities of the ice sheet at the mouth of Hudson strait. Each of the second or the third instability provokes large-scale surges (HEs). The rotation angle affects the frequency of small-scale instabilities, but does not affect general features of the oscillation.

In conclusion, the results of the ISMIP HEINO runs with rotated sediment areas show that the simulated internal oscillations (growth phase followed by large-scale surges) are a robust feature. Although some details of the results are influenced by the rotation angle, the general features of the oscillations are essentially unaffected. This result supports our claim that the oscillations are a physically real process rather than just a numerical artifact.

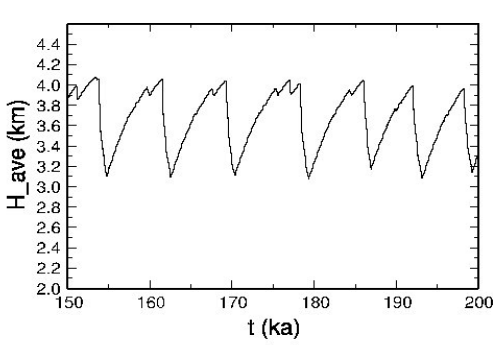

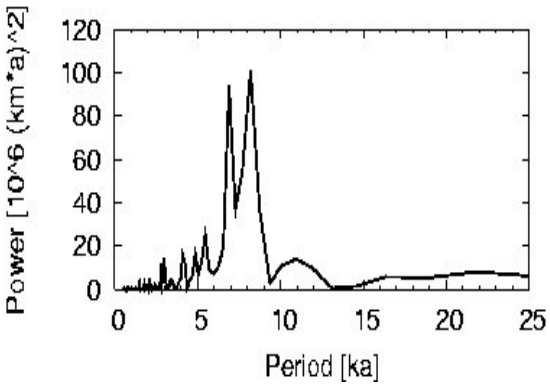

ST (a) (b)

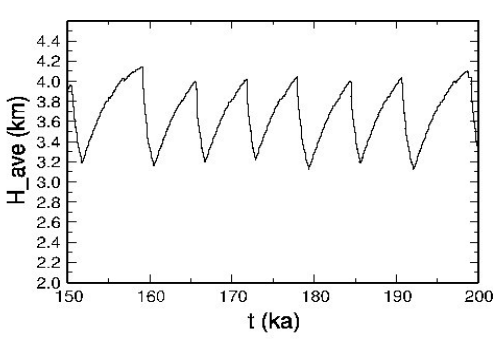

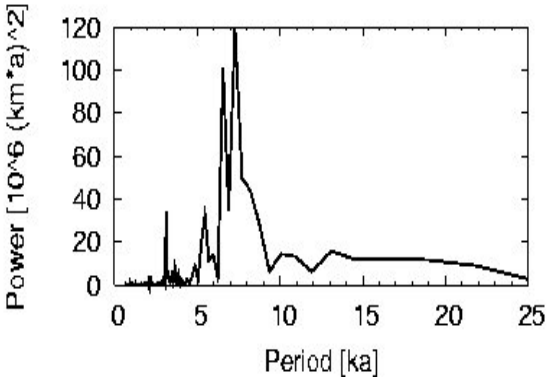

Str-05 (c) (d)

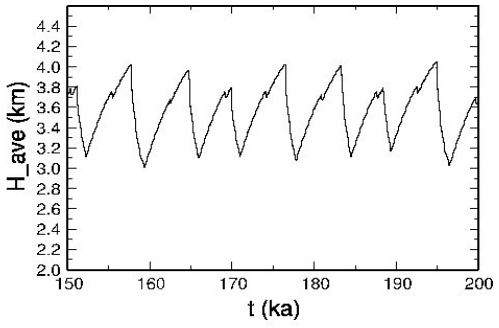

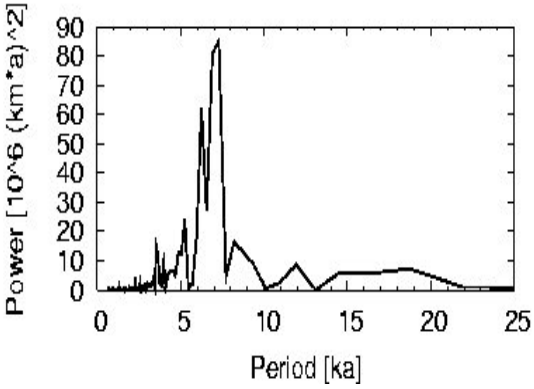

STr-10 (e) (f)

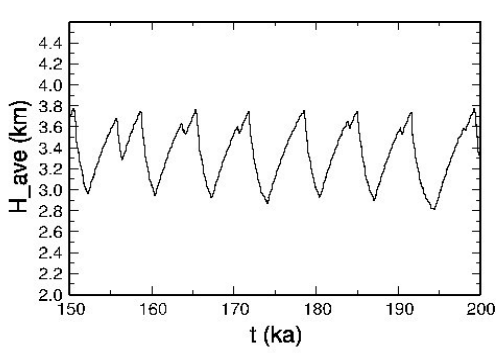

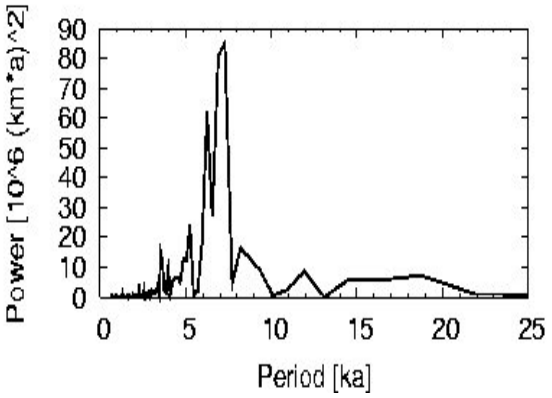

STr-15 (g) (h)

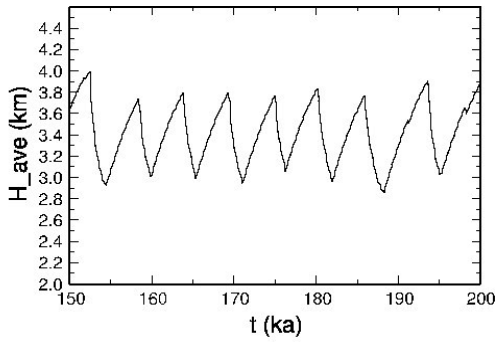

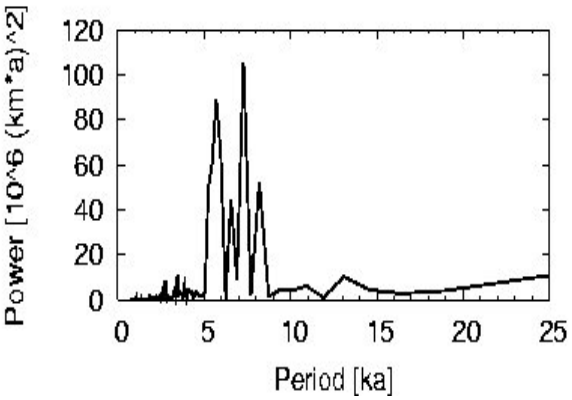

STr-20 (i) (j)

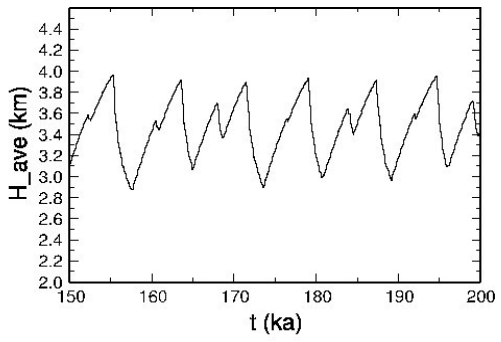

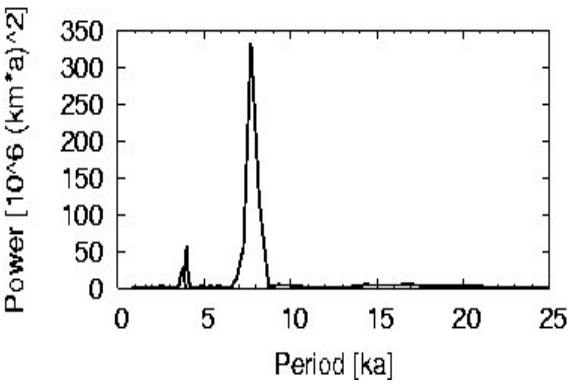

STr-25 (k) (l)

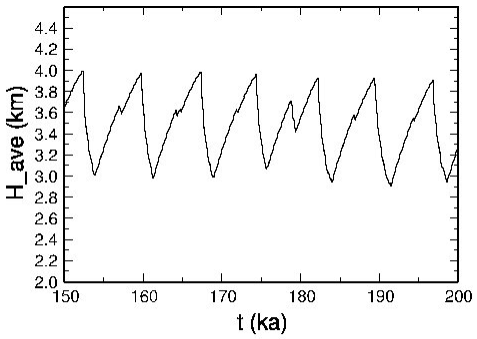

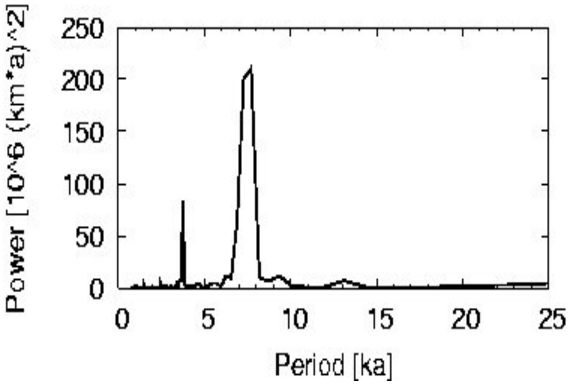

STr-30 (m) (n)

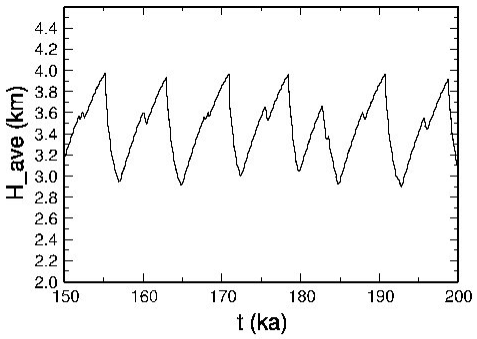

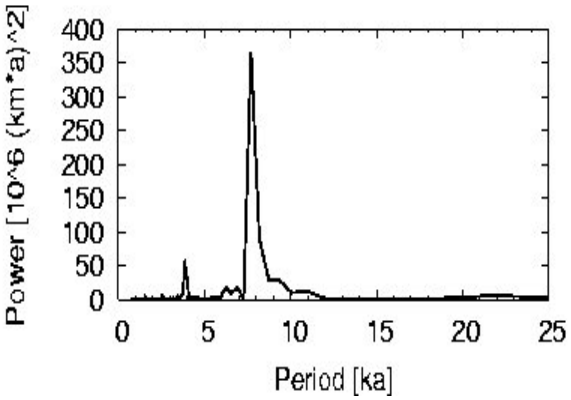

STr-35 (o) (p)

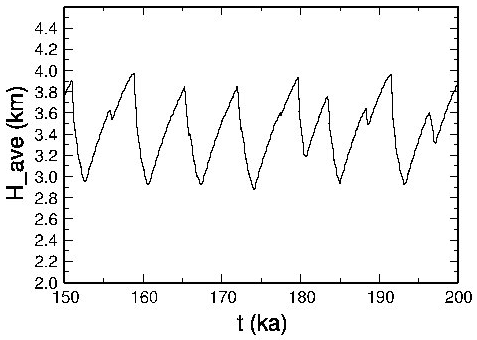

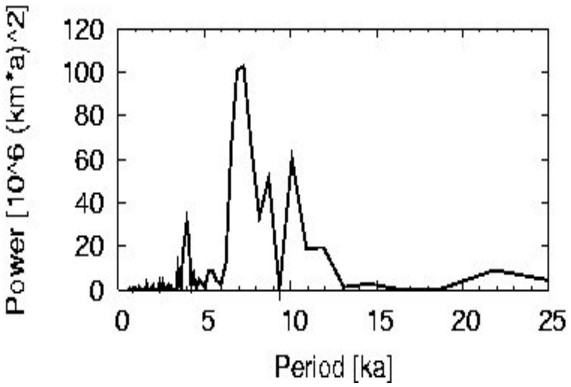

STr-40 (q) (r)

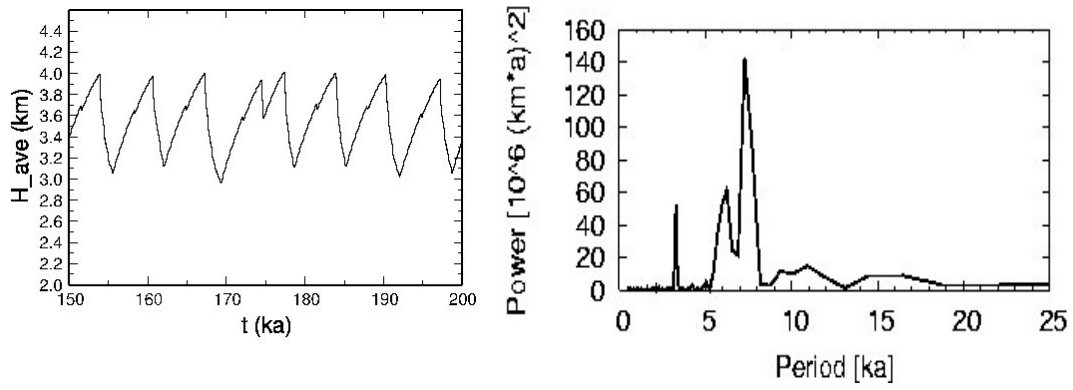

STr-45 (s) (t)

Fig. 4.9: Time series of average ice thickness, H_{ave}, and power spectrum for runs ST ((a), (b)), with STr-05 ((c), (d)), STr-10 ((e), (f)), STr-15 ((g), (h)), STr-20 ((i), (j)), STr-25 ((k), (l)), STr-30 ((m), (n)), STr-35 ((o),(p)), STr-40((q), (r)), and STr-45 ((s), (t)).

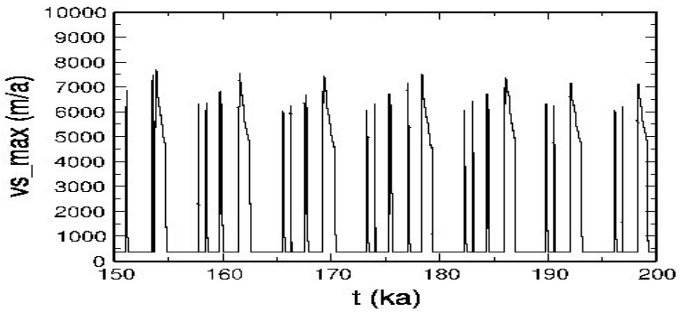

(a)

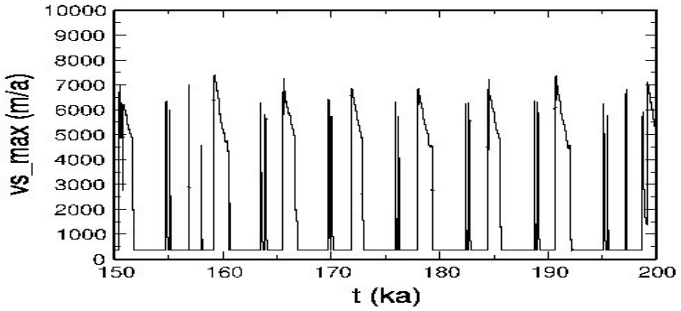

(b)

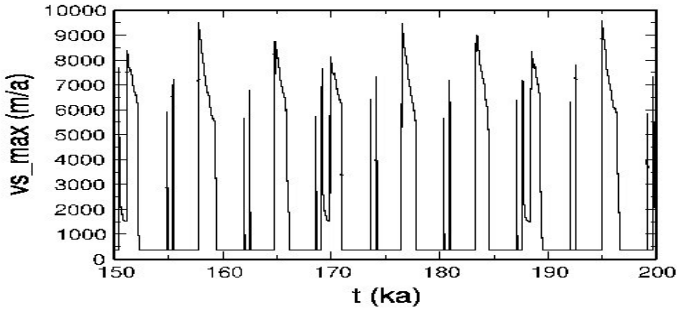

(c)

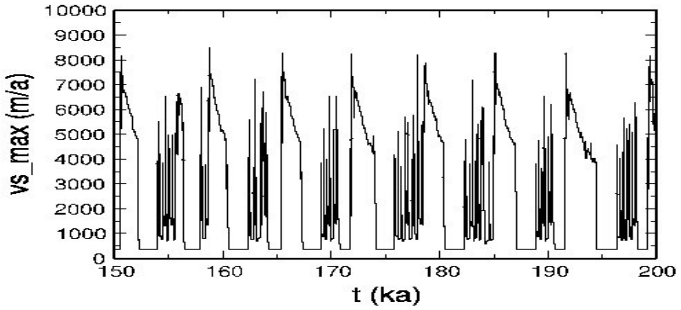

(d)

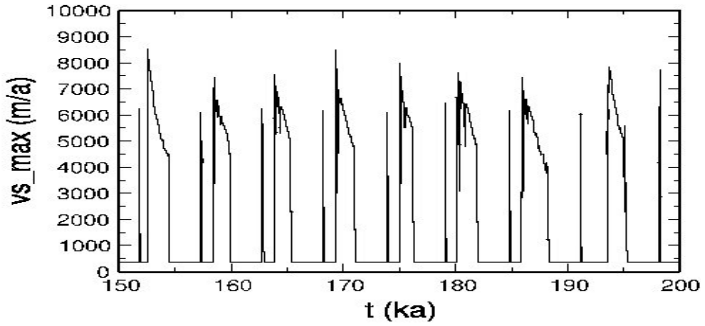
vs_max (m/a)
10000
9000
8000
7000
6000
5000
4000
3000
2000
1000
0
150
160
170
180
190
200
t (ka)

(e)

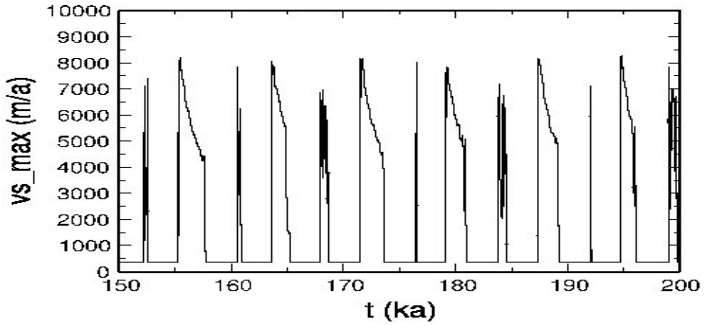
vs_max (m/a)
10000
9000
8000
7000
6000
5000
4000
3000
2000
1000
0
150
160
170
180
190
200
t (ka)

(f)

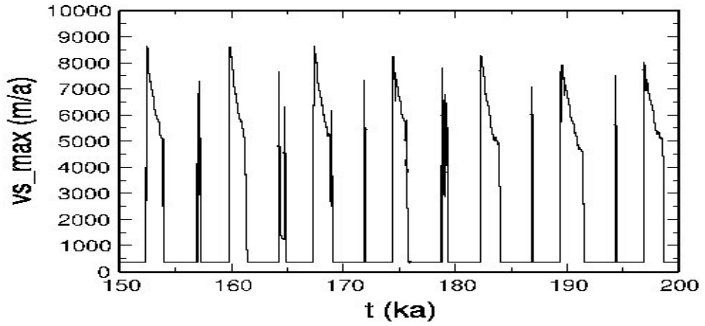
vs_max (m/a)
10000
9000
8000
7000
6000
5000
4000
3000
2000
1000
0
150
160
170
180
190
200
t (ka)

(g)

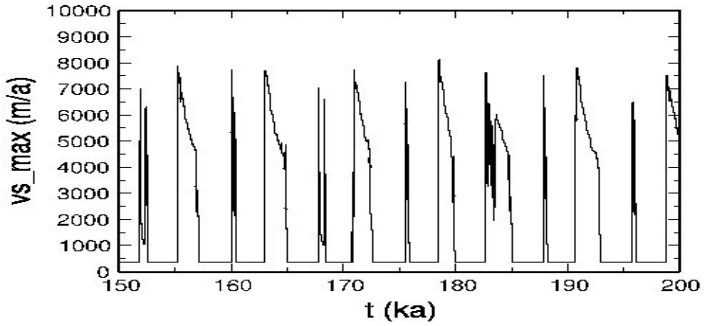

(h)

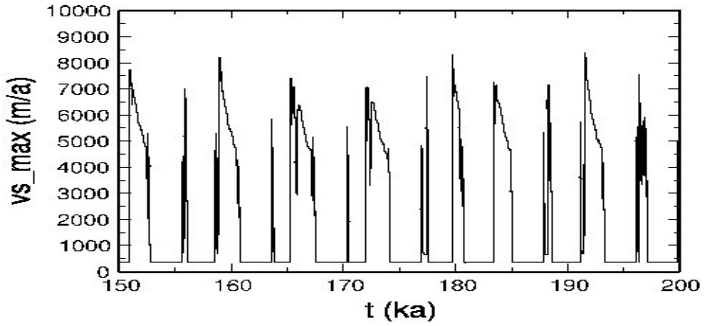

(i)

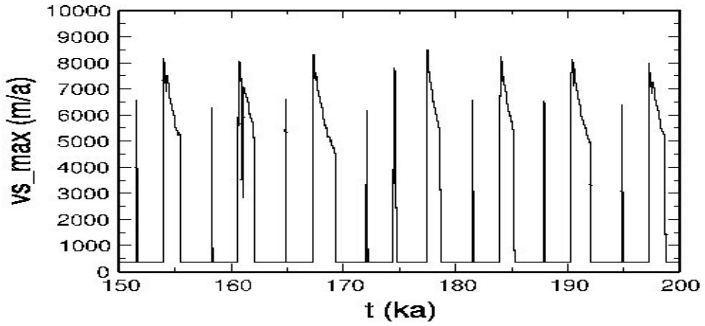

(j)

Fig. 4.10: Time series of maximum surface velocity over the land area during the last 50 kyr for runs ST (a), STr-05 (b), STr-10 (c), STr-15 (d), STr-20 (e), STr-25 (f), STr-30 (g), STr-35 (h), STr-40 (i), and STr-45 (j).

5. Summary and conclusions

HEs are large scale surges of the LIS over Hudson Bay and Hudson strait. It is important to investigate HEs in terms of glaciology as well as of climatology. In this study, it was tested whether the 3D ice sheet models SICOPOLIS (Greve., 1997) is able to simulate such large scale surges, and what is their sensitivity to changes of boundary conditions and to rotations of the domains of Hudson Bay and Hudson Strait.

We could produce internal ice-sheet oscillations (HEs) by SICOPOLIS. A full cycle consists of a slow growth phase (several kyr) followed by a rapid large-scale surge (HE, only some 100 years), and the mean period is about 7 kyr for run ST. We could also make sure that the HEs occur when the basal temperature reaches the pressure melting point, so that very rapid basal sliding on a lubricating sediment layer develops. During the HEs, flow velocities of up to 8 km/yr are developed. In addition to HEs, the signal of the maximum surface velocity shows a number of additional, higher frequency peaks, which are derived from small scale sediment slidings ('mini-HEs') at the mouth of Hudson Strait. The differences between HEs and 'mini-HEs' are the scale of collapse, ice velocity, and the period.

In changed boundary condition tests, the surface temperature affects the ice volume because it affects the ice thickness needed to trap enough internal heat to release a HE. The surface accumulation mainly affects the periodicity of HEs because it affects the growth time until the ice sheet gets sufficient thickness to trap enough internal heat. Further, the strength of subglacial sediment affected the amplitude of ice-volume changes because it affects ice velocities during the HEs. Therefore, surface and basal conditions of the LIS are crucial elements for HEs.

The results of run ST with rotated sediment area have shown that the simulated internal oscillations are a robust feature. While some details of the results depend on the rotation angle, the overall shape the oscillation is

essentially unaffected. This supports our claim that the oscillations are a physically real process rather than just numerical artifact.

6. References

1. Alley, R. B., Clark, P. U. The deglaciation of the Northern Hemisphere: a global perspective. *Ann. Rev. Earth Planet. Sci.*, 149-182 (1999).
2. Bond, G., Broecker, W., Johnson, S., McManus, J., Labeyrie, L., Jouzel, J., and Bonani, G. Correlation between climate records from North Atlantic sediments and Greenland ice, *Nature* **365**, 143-147, (1993).
3. Bond, G., Heinrich, H., Broecker, W., Labeyrie, L., McManus, J., Andrews, J., Huon, S., Jantschik, R., Clasen, S., Simet, C., Tedesco, K., Klas, M., Bonani, G., Lvy, S. Evidence for massive discharges of icebergs into the North Atlantic ocean during the last glacial period. *Nature* **369**: 245 – 249, (1992).
4. Bond, G., Broecker, W., Johnsen, S., Mcmannus, J., Labeyrie, L., Jouzel, J., Bonani, G. Correlations between climate records from North Atlantic sediments and Greenland ice. *Nature* **365**: 143-7 (1993).
5. Bond, G., Lotti, R. Iceberg discharges into the North Atlantic on millennial time scales during the last deglaciation. *Science* **267**, 1005-10 (1995).
6. Bond, G., Marchitto, T. M., McManus, J. F., Oppo, D. W., Laarkamp, K. L. American Geophysical Union. *Geophysical Monograph Series*, 1999, No.112, Mechanisms of Global Climate Change at Millennial Time Scales, edited by Clark. P. U, Webb. R. S, Keigwin. L. D, Eds (AGU, Washington, DC, 1999), pp. 35-58.
7. Calov, R., Ganopolski, A., Petoukhov, V., Claussen, M., Greve, R. Large-scale instabilities of the Laurentide ice sheet simulated in a fully coupled climate-system model. *Geophysical Research Letters*, **29** (24), 2216, doi: 10.1029 / 2002GL016078 (2002).
8. Calov, R., Greve, R. ISMIP HEINO ~ Ice Sheet Model Intercomparison Project - Heinrich Event INtercOmparison (2005).
9. Clark, P. U., Alley, R. B., David, P. Northern Hemisphere Ice-Sheet

Influences on Global Climate Change. *Science* **286**, 1104 – 1111 (1999).

10. Greve, R. Dynamics of Ice Sheets and Glaciers. Lecture notes, Institute of Low Temperature Science, Hokkaido University (2004 / 2005).
11. Greve, R. Relation of measured basal temperatures and the special distribution of the geothermal heat flux for the Greenland ice sheet. *Annals of Glaciology* Vol. **42** (in press, 2005).
12. Greve, R. A continuum-mechanical formulation for shallow polythermal ice sheets. *Phil. Trans. R. Soc. Lond.* A **355**, 921 - 974 (1997).
13. Hays, J, D., Imbrie, J. N., Shackleton, N. J. *Science* **194**, 1121 (1976); Imbrie. J et al., in Milankovitch and climate, part1, Berger. A. L et al., Eds (Kluwer Academic, Boston, MA, 1984), pp. 121-164.
14. Heinrich, H. Origin and consequences of cyclic ice rafting in the Northeast Atlantic Ocean during the past 130k years. *Quaternary Research*, **29**, 142-152 (1998).
15. Imbrie, J., Boyle, E. A., Clemens, S. C., Duffy, A., Howard, W. R., Kukla, G., Kutzbach, J., Martinson, D. G., McIntyre, A., Mix, A. C., Molfino, B., Morley, J. J., Peterson, L. C., Pisias, N. G., Prell, W. L., Raymo, M. E., Shackleton, N. J., Toggweiler, J. R. On the structure and origin of mjajor glaciation cycles. 1. Linear responses to Milankovitch forcing. *Paleoceanography,* **7**, 701-738 (1992).
16. Imbrie, J and 18 others. On the structure and origin of major glaciation cycles. 2. The 100,000-year cycle. *Paleoceanography,* **8**, 699-735 (1993).
17. Kawakami, S. Shima-shima-gaku (縞々学) pp. 118 – 119, University of Tokyo, Japan (1995).
18. Keigwin, L. D., Jones, G. A., Lehman, S. J. Deglacial meltwaterdischarge, North Atlantic deep circulation and abrupt climate change. *J. Geophys. Res.,* **96**, 16, 811 (1991).
19. Keigwin, L. D., Lehman, S. J. Deep circulation change linked to Heinrich event 1 and Younger Dryas in a middepth North Atlantic core, *Paleoceanography*, **9**, 185– 194 (1994).

20. Paterson, W. S. B. The Physics of Glaciers. Tarrytown, New York, pp.85 – 98, pp.133 – 172 (1994).
21. Saito, F. Development of a Three Dimensional Ice Sheet Model for Numerical Studies of Antarctic and Greenland Ice Sheet. Center for Climate System Research, University of Tokyo, Japan (2002).
22. Walder, J. S., Costa, J. E. Outburst floods from glacier-dammed lakes: The effect of mode of lake drainage on flood magnitude. *Earth Surf. Proc. Land*. **21**, 701 (1992).
23. Weertman, J. On the sliding of glaciers. *J.Glaciol*, **3**, 33 – 38 (1957).
24. Willson, R. C. L., Drury, S. A., Chapman, J. L. The Great Ice Age. Routledge, Great Britain (2000).